

## REVIEW

[View Article Online](#)  
[View Journal](#) | [View Issue](#)Cite this: *Energy Environ. Sci.*,  
2023, 16, 1364

## Recent advances in carbon-based nanomaterials for multivalent-ion hybrid capacitors: a review

Xuan Gao,<sup>ab</sup> Haoyu Wu,<sup>c</sup> Chang Su,<sup>d</sup> Chuanming Lu,<sup>d</sup> Yuhang Dai,<sup>b</sup> Siyu Zhao,<sup>b</sup> Xueying Hu,<sup>a</sup> Fangjia Zhao,<sup>a</sup> Wei Zhang,<sup>b</sup> Ivan P. Parkin,<sup>b</sup> Claire J. Carmalt<sup>\*a</sup> and Guanjie He<sup>id\*ab</sup>

Hybrid capacitors are emerging because of their ability to store large amounts of energy, cycle through charges quickly, and maintain stability even in harsh environments or at extreme temperatures. Hybrid capacitors with monovalent cations such as Li<sup>+</sup>, Na<sup>+</sup>, and K<sup>+</sup> have been extensively studied. However, the flammable nature of organic electrolytes and the reactive alkali metallic electrodes have raised safety concerns. This has prompted the development of novel aqueous multivalent cation storage systems, which can provide several benefits, including high capacity and energy density, rapid charge transfer, and low cost. With these advantages and the energy storage properties, multivalent cations such as Zn<sup>2+</sup>, Mg<sup>2+</sup>, Ca<sup>2+</sup>, and Al<sup>3+</sup> have been applied to multivalent-ion hybrid capacitors (MIHCs), and the latest developments and design ideas for these have been recently reviewed. However, an overview from the perspective of materials with unique advantages and experimental designs remains limited. Carbon-based nanomaterials are leading candidates for next-generation energy storage devices due to their outstanding properties in MIHCs. The use of carbon-based nanomaterials is attractive because these materials are inexpensive, scalable, safe, and non-toxic. They are also bioactive at the anode interface, allowing them to promote electrochemical reactions with redox species that would otherwise not take place. This paper reviews recent advances in MIHCs and related carbon-based materials and discusses the utilization of carbon materials in MIHCs and ideas for material design, electrochemical behavior, energy storage mechanisms, electrode design, and future research prospects. Based on the integration of related challenges and development, we aim to provide insights and commercialization reference for laboratory research. For the first time, combined with global intellectual property analysis, this paper summarizes the current main research institutions and enterprises of various hybrid capacitors, and provides important technical competition information and development trends for researchers and practitioners in the field of energy storage. Simultaneously, we provide a perspective for the development of MIHCs, a description of the existing research, and guidelines for the design, production, commercialization, and advancement of unique high-performance electrochemical energy storage devices.

Received 17th November 2022,  
Accepted 27th February 2023

DOI: 10.1039/d2ee03719j

[rsc.li/ees](http://rsc.li/ees)

### Broader context

This paper reviews recent advances in MIHCs and related carbon-based materials, discusses the utilization of carbon materials in MIHCs and ideas for material design, electrochemical behavior, energy storage mechanisms, electrode design, and future research prospects. Based on the integration of related challenges and development, we aim to provide insights and commercialization reference for laboratory research. In addition to summarizing the research progress in energy storage technology, materials science, *etc.*, the global commercialization of the energy storage field is also discussed. For the first time, combined with global intellectual property analysis, this paper summarizes the current main research institutions and enterprises of various hybrid capacitors, and provides important technical competition information and development trends for researchers and practitioners in the field of energy storage. Simultaneously, we provide a perspective for the development of MIHCs, a description of the existing research, and guidelines for the design, production, commercialization, and advancement of unique high-performance electrochemical energy storage devices.

<sup>a</sup> Christopher Ingold Laboratory, Department of Chemistry, University College London, 20 Gordon Street, London, WC1H 0AJ, UK. E-mail: [g.he@ucl.ac.uk](mailto:g.he@ucl.ac.uk), [c.j.carmalt@ucl.ac.uk](mailto:c.j.carmalt@ucl.ac.uk)<sup>b</sup> Department of Chemical Engineering, University College London, London, WC1E7JE, UK<sup>c</sup> School of Physics, Xi'an Jiaotong University, No. 28, Xianning West Road, Xi'an, 710049, China<sup>d</sup> Nanyang Technopreneurship Center, Nanyang Technological University, 50 Nanyang Avenue, Singapore 639798, Singapore

## 1. Introduction

Due to the rapid emergence and increasing popularity of electric vehicles and portable electronics, energy storage devices have gained considerable attention. Over the last few decades, supercapacitors have emerged as one of the most exciting new battery technologies.<sup>1–3</sup> Unlike conventional batteries, which store energy by means of chemical reactions, supercapacitors can be charged and discharged almost instantly, and can deliver sufficient power rapidly.<sup>4–7</sup> Since supercapacitors are less expensive and lighter in weight than batteries, they have the potential to be employed in a wide range of applications. Their high charge–discharge rate, long service life, and broad application temperature range make them ideal for various electrical and electronic systems.<sup>8</sup> However, poor energy density significantly restricts their scalability.

By combining the advantages of batteries with supercapacitors, hybrid capacitors are suggested as alternative technologies. Hybrid capacitors are emerging because of their ability to store large amounts of energy, cycle through charges quickly, and maintain stability even in harsh environments or at extreme temperatures.<sup>9</sup> Electrode materials with different features are used, one of which demonstrates electrostatic capacitance, while the other primarily demonstrates electrochemical

capacitance. The electrolyte creates an ionically conductive medium between the two electrodes. Hybrid capacitors with monovalent cations such as  $\text{Li}^+$ ,  $\text{Na}^+$ , and  $\text{K}^+$  have been extensively studied. However, the flammable nature of organic electrolytes and the reactive alkali metallic electrodes have raised safety concerns. This has prompted the development of novel aqueous multivalent cation storage systems which can provide several benefits, including high capacity and energy density, rapid charge transfer, and low cost.<sup>10</sup>

With these advantages, the energy storage mechanism of multivalent cations ( $\text{Zn}^{2+}$ ,  $\text{Mg}^{2+}$ ,  $\text{Ca}^{2+}$ , and  $\text{Al}^{3+}$ ) has been applied to multivalent-ion hybrid capacitors (MIHCs), and the latest developments and design ideas for these have been recently reviewed.<sup>11–13</sup> However, an overview from the perspective of materials with unique advantages and experimental designs remains limited. Carbon-based nanomaterials are leading candidates for next-generation energy storage devices due to their outstanding properties in MIHCs. The use of carbon-based nanomaterials is attractive because these materials are inexpensive, scalable, safe, and non-toxic while also being bioactive at the anode interface, which allows them to promote electrochemical reactions with redox species that would not otherwise take place.<sup>14</sup>

In fact, various energy storage technologies with metal cations as charge carriers are at different stages in the industry. Patents are legally protected against the copying of proprietary technology by competitors and provide a strong safeguard for commercialization. Hence, patents can reveal the current status of technological development effectively. Fig. 1 displays the patent analysis of different energy storage technologies with different charge carriers and the institutes or companies that currently hold the most patents for the corresponding technologies. As shown in Fig. 1, Li-ion energy storage techniques, which were on an upward trend from 2012, have gradually declined from 2017 onwards. Japanese companies (e.g., Toyota Motor Corporation, Panasonic Holdings Corporation, and Semiconductor Energy Laboratory) are the leaders in the industrial application of this technology. The Na-ion energy storage technology is the second most mature technology after lithium, with 3440 patents being recorded for the technology over the



**Xuan Gao**

*Xuan Gao is currently pursuing a PhD at University College London (UCL) after completing his Master's degree at the National University of Singapore (NUS). He has worked as a national senior scholar at the Department of Operations Support in the United Nations. His current research focuses on aqueous zinc-ion batteries, nanomaterials, multivalent cation batteries, etc.*



**Claire J. Carmalt**

*Prof. Claire J. Carmalt is a British chemist who is a professor of inorganic chemistry and Head of the Department of Chemistry at UCL. Her research considers the synthesis of molecular precursors and the development of thin film deposition techniques. She received multiple awards including the 2019 Royal Society of Chemistry Applied Inorganic Chemistry Award and 2018 Ramsay Trustee of the Society of Chemical Industry.*



**Guanjie He**

*Dr Guanjie He is an assistant professor in the Department of Chemical Engineering, UCL. His research fields are mainly aqueous batteries, electrocatalytic materials and devices, advanced characterization and simulation. He has published more than 100 scientific research papers and received the ERC starting grant, EPSRC New Investigator Award on aqueous energy storage research.*





Fig. 1 Patent overview of different energy storage technologies.

last decade. However, most of the patents are held by Chinese universities, reflecting the fact that Chinese companies have not yet commercialized sodium ion energy storage technology to a high degree. Similar to Li-ion energy storage technology, Japanese companies (*e.g.*, Panasonic Co., Ltd, Semiconductor Energy Laboratory, and HITACHI) have the majority of patents in Zn-ion energy storage technology, as depicted in Fig. 1. Interestingly, this technology doubled in 2017 and 2019, with declining trends in the other years. China and the USA have mastered K-ion energy storage technology with comparable strength. However, while in the US, the technology is mainly

held by companies, in China, it is still held by universities and research institutions. In contrast, Japanese companies keep leading the way in Mg-ion energy storage technologies, however, the available patents are not huge in number for this technology as a whole. Aluminum-ion energy storage technology is another developing area. The Netherlands mastery of the technology is impressive, while Japan and the USA also contributed to this technology. Finally, the development of Ca-ion energy storage technology is the slowest of all until now. Only 1200 technological patents have been granted in the last decade, which is in contrast to the number of patents for other



cationic energy storage technologies. The competition for this technology is fierce, and various countries (*e.g.*, UK, USA, Japan, China, and Germany) are actively involved.

The most recent developments in MIHCs and related carbon-based materials are reviewed herein. The integrated characteristics of hybrid capacitors, related to the structures and mechanisms of MIHCs are covered first. Then the application of carbon materials in MIHCs is explained, including the types of carbon materials, material design concepts, electrochemical behaviors, energy storage mechanisms, electrode designs, and future research directions. In addition to a summary of existing research, we present an outlook for the development of MIHCs and give the direction for the design, manufacture, and development of high-performance electrochemical energy storage devices.

## 2. Design mechanism of MIHCs

Since MIHCs are designed based on the mechanism of supercapacitors and multivalent cation batteries, as shown in Fig. 2, the structures and mechanisms of supercapacitors and multivalent cation batteries are discussed first.

### 2.1. Concepts of supercapacitors and multivalent cation batteries

**2.1.1. Supercapacitors.** Electric double-layer capacitors (EDLCs) and pseudo-capacitors are two kinds of supercapacitors that are presently being investigated the most in terms of their varied energy storage mechanisms, as shown in Table 1. The energy storage mechanism of an EDLC is mostly dependent

on the electric double layer produced at the interface of each electrode and electrolyte in order to complete the electrostatic adsorption and desorption processes. This process is physical and thus, the formed electric double layer is extremely stable and generates a stable potential between the electrodes, providing high power densities and stable cycling performance. Faradaic capacitors, also called pseudo-capacitors, generate capacitance due to the occurrence of rapid reversible chemical adsorption/desorption or redox reactions at the electrodes. Compared with EDLCs, pseudo-capacitors have higher energy density. However, the charge/discharge power and cycle life of pseudo-capacitors are lower than those of EDLCs owing to the electrochemical reaction kinetics and the unavoidable irreversibility of the reaction throughout the cycle.

**2.1.2. Multivalent cation batteries.** Multivalent cations are the charge carriers shuttling between the cathode and anode during the discharging and charging process without causing drastic changes in the composition of the electrolyte solution. This is an example of a rocking chair type battery, which is similar to Li-ion batteries.<sup>15</sup> The motivations for carrying out more research on multivalent cation batteries include the demand for new energy storage technologies because of the continuous rise in the price of lithium resources, and the use of relatively inactive metals as safe anodes. The working principle of multivalent cation batteries is similar to that of Li-ion batteries, which means that the basic understanding and manufacturing experiences accumulated for Li-ion batteries are available, which accelerates the industrial adaptation of multivalent cation batteries. Multivalent cation batteries based on divalent zinc ions, magnesium ions, calcium ions, and trivalent aluminum ions are being widely studied. However,



Fig. 2 Mechanisms of supercapacitors, batteries and hybrid capacitors.



Table 1 Comparison of the advantages and disadvantages of electric double-layer capacitors and pseudo-capacitors

| Item                             | EDLCs   | Pseudo-capacitors   |
|----------------------------------|---|---|
| Electrode material               | Carbon materials  | Transition metal oxides, conducting polymers, and hydroxides, <i>etc.</i>                                     |
| Electrode with chemical activity | No  | Yes   |
| Energy storage mechanism         | Physical absorption   | Redox reaction  |
| Advantages                       | Stable performance in long-term cycle<br>Fast charge and discharge<br>High power density<br>Wide operating temperature window | High specific capacitance ( $> 1000 \text{ F g}^{-1}$ )<br>High energy density ( $> 35 \text{ W h kg}^{-1}$ ) |
| Disadvantages                    | Low energy density ( $< 15 \text{ W h kg}^{-1}$ )   | Lack of stability during cycle  |

their development also depends on whether multivalent metals bring enough benefits over lithium to be worthy of consideration as a substitute. As shown in Fig. 3a, compared with lithium-based anodes, the oxidation–reduction potential of multivalent metals is generally lower, which is also a problem faced by researchers currently and they are making efforts to

overcome it. However, multivalent cation batteries have a higher volumetric energy density than monovalent cation batteries, which is an advantage for next generation energy storage technology. In addition to competing with mature Li-ion batteries, various multivalent cation batteries have also become internal technical competition.

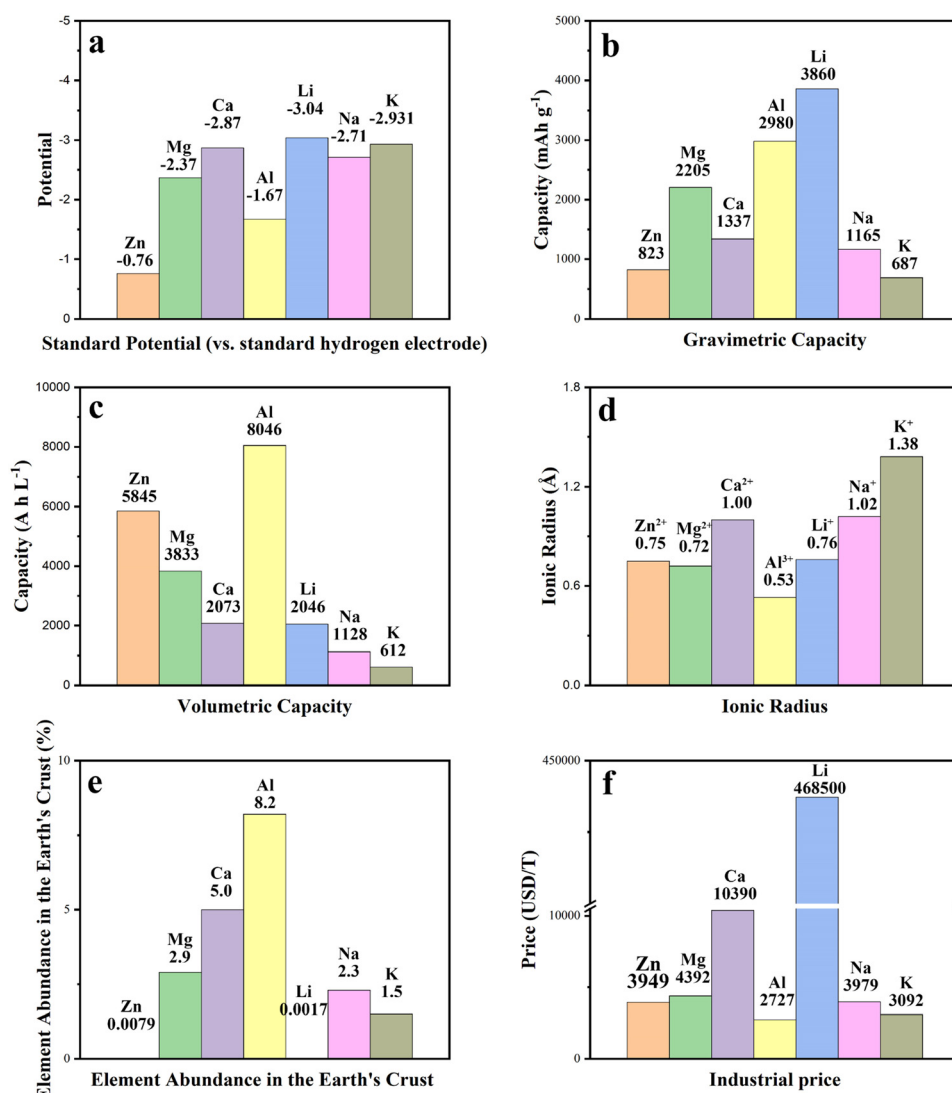


Fig. 3 (a) Standard potential (vs. standard hydrogen electrode), (b) gravimetric capacity, (c) volumetric capacity, (d) ionic radius, (e) abundance in the earth's crust, and (f) raw material cost of multivalent metal elements zinc, magnesium, calcium, aluminum and monovalent metal elements lithium, sodium, and potassium.



## 2.2. Concept of multivalent-ion hybrid capacitors

Supercapacitors have excellent characteristics, such as fast charging rates and long service life, however, their power density is low, which limits the industrial application of supercapacitors. Multivalent cation batteries have a high energy density, but their output power and cycle stability have also defined their application range. MIHCs combine the advantages of both and circumvents the disadvantages of supercapacitors and multivalent cation batteries through the combination of battery-type electrodes and capacitor-type electrodes. When the capacitor-type electrode acts as the cathode of MIHCs and the battery-type electrode acts as the anode of MIHCs, the cathode acquires an electric double layer (EDL) or Faradaic intercalation occurs during charging, while anions and high-valent metal cations diffuse back into the electrolyte during discharge. When the capacitor-type electrode is used as the anode of MIHCs and the battery-type electrode is used as the cathode of MIHCs, the adsorption of high-valent cations on the battery-type cathode enables the MIHCs to have a high power density.

MIHCs has several advantages over conventional supercapacitors and multivalent cation batteries. First, MIHCs exhibit high energy densities, similar to batteries, and high power densities, similar to supercapacitors. This combination makes them suitable for applications that require both high energy and high power delivery, such as electric vehicles and renewable energy storage. Second, MIHCs use multivalent ions, such as zinc, magnesium or aluminum, in the electrolyte, which results in faster charging and discharging compared to traditional supercapacitors that use only monovalent ions. MIHCs also have longer cycle lives than traditional supercapacitors, as they are not limited by the same capacitance fading mechanisms. Furthermore, MIHCs can be made safer than batteries due to the use of non-flammable electrolytes and the absence of high voltage, which reduces the risk of thermal runaway and short-circuit events. Additionally, MIHCs can be made more environmentally friendly compared to batteries by using biodegradable materials and reducing the use of heavy metals.

## 2.3. Electrolytes

Electrolytes are usually divided into aqueous and nonaqueous, as described below, and play an important role in improving electrode reaction efficiency and increasing the reaction rate. Improving the ionic and electronic conductivity of electrolytes is one of the current research focuses of researchers, which affects the reversible capacity and cycle stability of MIHCs.

**2.3.1. Aqueous electrolytes.** Aqueous electrolytes have been utilized in MIHCs because they are more ecologically friendly, safer, and less costly than nonaqueous electrolytes. Some inorganic salts with anions  $\text{SO}_4^{2-}$ ,  $\text{NO}_3^-$ ,  $\text{Cl}^-$ ,  $\text{CH}_3\text{COO}^{2-}$ ,  $\text{CF}_3\text{SO}_3^{2-}$ , *etc.* are commonly used as electrolytes for aqueous MIHCs due to their high conductivity, low cost, and environmental friendliness. Due to the fact that ions migrate more quickly in water, aqueous electrolytes may provide a larger ionic concentration and lower resistance, hence improving the rate performance of the devices.

In 2021, a novel redox bromide-ion additive aqueous Mg-ion hybrid capacitor (MHC) was proposed by inserting the  $\text{Br}^{3-}/\text{Br}^-$  redox additive into 1 M  $\text{MgSO}_4$  electrolyte in an effort to increase its energy density.<sup>16</sup> The designed hybrid capacitor has a maximum specific capacity of  $268.1 \text{ mA h g}^{-1}$  at a current density of  $2 \text{ A g}^{-1}$  across a broad voltage range of 2.6 V. (0–2.6 V). In addition, a maximum energy density of  $262.3 \text{ W h kg}^{-1}$  may be attained at a power density of  $1956.8 \text{ W kg}^{-1}$ . In the field of Zn-ion hybrid capacitors (ZHCs), Wu *et al.* studied the electrochemical characteristics of aqueous Zn-ion energy storage technology related to the electrolyte type and concentration.<sup>17</sup> The average Coulombic efficiency (CE) of Zn stripping/plating was determined to be as follows:  $\text{Zn}(\text{CF}_3\text{SO}_3)_2 \rightarrow \text{Zn}(\text{CH}_3\text{COO})_2 \rightarrow \text{ZnCl}_2 \rightarrow \text{ZnSO}_4 \rightarrow \text{Zn}(\text{NO}_3)_2$ , as shown in Fig. 4. Additionally, the electrolyte concentration had a noticeable influence on the CE of ZHCs, with the CE rising as the electrolyte concentration rises. The highest CE of Zn stripping/plating was achieved with  $\text{Zn}(\text{CF}_3\text{SO}_3)_2$  electrolyte at concentrations of 3 to 4 M. This is due to the higher interaction between  $\text{H}_2\text{O}$  and  $\text{CF}_3\text{SO}_3^-$  anions than between  $\text{Zn}^{2+}$  cations and  $\text{H}_2\text{O}$ , which limits the generation of by-products during zinc plating procedures.

**2.3.2. Nonaqueous electrolytes.** Nonaqueous electrolytes, such as organic and ionic liquid electrolytes, have recently attracted increased interest. Compared with aqueous electrolytes, organic or ionic liquid electrolytes exhibit a broader working potential window, resulting in a higher energy density.

**2.3.2.1. Organic electrolyte.** In 2021, Wang *et al.* proposed ZHCs with a nonaqueous electrolyte which achieved high cathode mass loading and high anode zinc utilization rates while maintaining a high capacity.<sup>18</sup> The proposed ZHCs consist of a porous carbon cathode generated from a metal organic framework (MOF), a metallic zinc anode, and *N,N*-dimethylformamide (DMF) electrolyte containing  $\text{Zn}^{2+}$ . The cathode's charge storage occurs mainly in macropores, demonstrating good rate performance under high mass loading. The DMF-based electrolyte may help in smooth deposition, permitting dendrite-free Zn plating/stripping, while its aprotic nature avoids unwanted  $\text{H}_2$  evolution. It was determined that the majority of the charge storage of the MOF-derived porous carbon cathode was due to anion and cation adsorption/exchange in macropores, as shown by *in situ* attenuated total reflection-Fourier transform infrared spectroscopy (ATR-FTIR). As a result, the capacitor exhibits stability after 9000 cycles and a zinc utilization rate of 2.2%. With a high mass loading of  $40 \text{ mg cm}^{-2}$ , the energy density approached  $25.9 \text{ W h kg}^{-1}$ . DMF-based electrolytes provide a feasible solution for capacitors operating at both high and low temperatures (−65 to  $100 \text{ }^\circ\text{C}$ ).

**2.3.2.2. Ionic liquid electrolytes.** Recently, trifluoromethanesulfonyl (TFSI<sup>−</sup>) has been commonly used in ionic liquid electrolytes. Tobias *et al.* proposed the reversible (de)intercalation of TFSI anions from a Mg-based ionic liquid electrolyte,  $\text{Mg}(\text{TFSI})_2$  in  $\text{Pyr}_{14}\text{TFSI}$ , within graphite/activated carbon hybrid dual-ion capacitors (DICs).<sup>19</sup> The Mg-based DICs were compared to cells with pure  $\text{Pyr}_{14}\text{TFSI}$  and  $\text{LiTFSI-Pyr}_{14}\text{TFSI}$





Fig. 4 Characterization of the Zn plating behavior in electrolytes containing different Zn salts. (a) XRD patterns and (b–f) SEM images of pristine Zn and Ti foils, and Ti foils with Zn layer plated in different 1 M Zn salts. (g) CEs of Zn stripping/plating in electrolytes containing different 1 M zinc salts. (h) CEs in Zn(CF<sub>3</sub>SO<sub>3</sub>)<sub>2</sub> electrolyte of different concentrations, inset: magnified view of the first 100 cycles denoted by grey dashed lines.<sup>17</sup> Reused with permission from Wiley.

electrolytes (Pyr<sub>14</sub>: *N*-butyl-*N*-methylpyrrolidinium), as well as graphite//Li metal dual-ion cells with LiTFSI-Pyr<sub>14</sub>TFSI electrolytes. At 5.2 V vs. Li/Li<sup>+</sup>, Mg-containing DIC cells outperform Li-based cells, exhibiting a greater capacity (87 vs. 85 mA h g<sup>-1</sup>) and better CE (98 vs. 96%). These findings may pave the way for more research on and performance enhancements of Mg-based energy storage technology, as well as hybrid DIC chemistry with other cations, particularly multivalent cations.

With TFSI anions, Li *et al.* developed a new non-aqueous electrolyte (Zn(TFSI)<sub>2</sub>/Pyr<sub>14</sub>TFSI/AN) based on acetonitrile (AN) combined with ionic liquids (Pyr<sub>14</sub>TFSI) and Zn(TFSI)<sub>2</sub>.<sup>20</sup> According to the study, the Raman spectral peaks changed dramatically with addition of 4 and 6 wt% AN. In the electrolyte containing 4 wt% AN, the free AN fraction predominates in comparison to the quantity of Zn<sup>2+</sup>-bound AN, while the electrolyte containing 6 wt% AN exhibits a reverse relationship.

Additionally, the findings illustrate the development of a Zn<sup>2+</sup> solvated structure. The coordination number of Zn-TFSI fell from 3.897 to 3.593 as the AN amount increased, but the coordination number of Zn-AN grew from 0.1 to 0.403. Simultaneously, the frequency of AN molecules in the initial solvation shell of Zn<sup>2+</sup> increased steadily as the quantity of AN increased. As a result, the coordination number of Zn-AN increased as the quantity of AN increased. This indicates a competition between TFSI<sup>-</sup> and AN molecules, as well as a significant interaction between the AN molecules and Zn<sup>2+</sup> in the hybrid electrolyte.

### 3. Classification of MIHCs

Hybrid capacitors are designed to have the most significant qualities of supercapacitors, namely, high-power capability and



extended cycle life, while having a better specific energy density than symmetric supercapacitors, which have solely electrostatic interactions between two electrodes. Typically, this is accomplished by building an asymmetric cell with an EDLC electrode and a redox battery electrode. The ideal case is that the specific capacitance of a battery electrode ( $C_{\text{BATT}}$ ) is semi-infinite. As a result, the EDLC electrode dominates the full-cell specific capacitance ( $C_{\text{tot}}$ ) of a hybrid capacitor. EDLC electrodes are often constructed from high surface area activated carbon (AC), and hence their capacitance may be approximated from the specific capacitance of the activated carbon ( $C_{\text{AC}}$ ) from which they are constructed. As a result, the hybrid, asymmetric supercapacitor's specific capacitance,  $C_{\text{tot}}$ , is comparable to that of AC. This follows the formula:

$$1/(m_{\text{tot}}C_{\text{tot}}) = 1/(m_{\text{AC}}C_{\text{AC}}) + 1/(m_{\text{BATT}}C_{\text{BATT}})$$

where  $m_x$  denotes the mass of component  $x$ .

For symmetrical supercapacitors, on the other hand,  $C_{\text{tot}}$  is restricted to  $0.25C_{\text{AC}}$  according to the following formula:  $1/(m_{\text{tot}}C_{\text{tot}}) = 2/(m_{\text{AC}}C_{\text{AC}})$ , where  $m_{\text{tot}}$  equals 2 times  $m_{\text{AC}}$  in this instance. As a result, hybrid capacitors have a higher  $C_{\text{tot}}$  than symmetrical supercapacitors.

### 3.1. Classification by multivalent ion

**3.1.1. Zn-ion hybrid capacitors.** Researchers have investigated MIHCs intensively, especially in ZHCs, in recent years because of their cheap cost, high safety, environmental friendliness, good electrochemical performance, and large theoretical capacity. As shown in Fig. 3a, compared to standard hydrogen electrodes, the redox potential of metallic zinc is ( $-0.76$  V). More importantly, a high theoretical gravimetric capacity of  $823 \text{ mA h g}^{-1}$  and a high volumetric capacity of  $5845 \text{ A h L}^{-1}$  make ZHCs a promising prospect. However, zinc has the same defects as the atoms of other multivalent metals, and the weight energy density of zinc is slightly lower than that of lithium metal. Some researchers have also proposed that the volumetric energy density exhibited by the application of  $\text{Zn}^{2+}$  in energy storage should not be too high. However, with the continuous research and development of electrodes and electrolytes, ZHCs are still a promising technology, which will have a certain share in the future energy technology competition. The research progress and design of ZHCs will be systematically discussed in Sections 3.2 and 3.3.

**3.1.2. Mg-ion hybrid capacitors.** MHCs have superior electrochemical performance due to high energy density, large capacities, and rapid charge transfer kinetics. What is more noteworthy is that magnesium is a unique active metal for battery-type electrodes in hybrid capacitors, having a volumetric capacity of  $3833 \text{ mA h cc}^{-1}$  (much higher than that of lithium of  $2046 \text{ mA h cc}^{-1}$ ). Additionally, the electrochemical deposition of magnesium does not create dendrites, which is a key concern when using other metallic anodes in rechargeable devices.<sup>21</sup>

MHCs are still in their infancy, due to the issue of passivation coatings forming on the surface of the metallic magnesium anode in electrolytes. This issue precludes the long-term

reversible deposition/dissolution of  $\text{Mg}^{2+}$  ions and so limits the practical use of MHCs. Due to the fact that the passivation films created on magnesium anodes are impermeable to  $\text{Mg}^{2+}$  ions, reversible magnesium deposition/dissolution requires solutions based on ether solvents and magnesium organo-haloaluminate complex electrolytes without forming passivation films on magnesium electrodes. Compatibility concerns make it difficult to match these complicated electrolyte solutions with cathodes; the magnesium organo-haloaluminate electrolytes are often nucleophilic and chemically reactive with electrophilic oxide electrodes. Additionally, due to the large ionic size of the magnesium ionic complexes, cathodes made using porous carbon cannot be used in the magnesium organo-haloaluminate electrolytes. As a result, proper electrode materials and electrolytes, as well as thorough investigation, are critical.

In 2022, Pan *et al.* developed an MHC with high capacity and stability based on expanded layer spacing  $\text{MoS}_2$  (E- $\text{MoS}_2$ ) nanosheet anodes.<sup>22</sup> The authors demonstrated that expanded layer spacing reduced ion diffusion resistance and offered more active sites so that  $\text{MoS}_2$  with expanded interlayer spacing was a prospective negative electrode material for rechargeable MHCs. The E- $\text{MoS}_2$ -based MHC exhibited an advantageous specific capacitance of  $274.2 \text{ F g}^{-1}$  at  $0.5 \text{ A g}^{-1}$  and a high energy density of  $192.8 \text{ W h kg}^{-1}$  at a power density of  $1682.7 \text{ W kg}^{-1}$ . Notably, the proposed MHC demonstrated superior long-term capacity retention, retaining 93.8% of its capacitance after 30 000 cycles. The enhanced capacity and stability were attributed to the increased number of active sites for  $\text{Mg}^{2+}$  storage and the decreased ion diffusion resistance provided by the expansion of the  $\text{MoS}_2$  layer spacing.

**3.1.3. Ca-ion hybrid capacitors.**  $\text{Ca}^{2+}$  has superior kinetics compared to other multivalent chemistries due to its moderate charge density and polarization strength, which translates into a greater power advantage.  $\text{Ca}^{2+}$  energy storage technology, when combined with its abundance (2500 times that of lithium), has the potential to produce high-capacity, high-power, and low-cost devices. However, the electrochemical performances of previously described  $\text{Ca}^{2+}$  hybrid capacitors (CHCs) remain unsatisfactory for practical applications. Research on CHCs has shown a decreasing trend in recent years although discussions on the development of  $\text{Ca}^{2+}$  energy storage devices have been ongoing for three decades. Aurbach *et al.* stated for the first time in 1991 that Ca deposition in organic solutions is impossible at room temperature. Aurbach believed that, although molten salt cells have been shown to be highly reversible at extreme operating temperatures ( $550\text{--}700$  °C), they were difficult to achieve in room temperature applications.

It has been challenging to create Ca-based energy storage devices based on the standard rocking-chair mechanism due to the lack of an ideal mix of compatible electrode materials and electrolytes. Direct application of metallic calcium anodes falls short of achieving the criteria of commercialization, especially showing a poor CE in low-power state. The reversibility of metallic calcium anodes is limited because of the creation of a passivation layer during the oxidation of  $\text{Ca}^{2+}$ . Sn is utilized as



the battery electrode in the majority of Ca energy storage systems. Sn combines with  $\text{Ca}^{2+}$  during the process to generate a Ca–Sn alloy ( $\text{Ca}_7\text{Sn}_6$ ). When the alloy interacts, the electrons exhibit fast transmission.

Tang *et al.* deconstructed the basic challenge-confronting calcium-based energy storage devices and established a multi-ion reaction method necessary to develop a full device.<sup>23</sup> To develop a comprehensive Ca-ion energy storage device, a multi-ion reaction method was devised, and a capacitor–battery hybrid mechanism was purposefully chosen. To achieve a longer life span, quicker kinetics, increased capacity, and higher voltage, a capacitor–battery hybrid mechanism was used to build a hybrid Ca-ion energy storage device at ambient temperature using typical organic electrolytes. Due to the intricate design, it has a good reversible capacity of  $92 \text{ mA h g}^{-1}$  after 1000 cycles.

**3.1.4. Al-ion hybrid capacitors.** In comparison to Li resources, Al is available around the planet at a far cheaper cost. Rechargeable Al-ion batteries with ionic liquid and aqueous electrolytes have just recently become available. There are, however, very few investigations on Al-ion hybrid capacitors (AHCs). The primary reason for this is that suitable electrochemical performance electrode materials for AHC are scarce.

Meanwhile, AHCs have long been constrained in their kinetics and reversibility by the high electrostatic field around the bare  $\text{Al}^{3+}$ . While using hydrated  $\text{Al}^{3+}$  as charge carriers may alleviate this problem, their huge size puts stringent restrictions on the pore architecture of electrode materials. Qu *et al.* devised an adaptive pore-structure remolding technique for capacitive electrode materials in order to achieve very compact and orderly storage of hydrated  $\text{Al}^{3+}$ .<sup>24</sup> The cathode was made by graphene-based remolding of highly ordered and compact porous carbon (RHOPC) and the anode was made by remolding alkali-treated  $\text{Ti}_3\text{C}_2\text{T}_x$  (RAT- $\text{Ti}_3\text{C}_2\text{T}_x$ ). The proposed AHC demonstrated a high operating voltage of up to 2.0 V, an energy density of  $112 \text{ W h L}^{-1}$ , and a power density of  $30\,000 \text{ W L}^{-1}$  after 10 000 cycles.

### 3.2. Classification by configuration

From the configuration point of view, MIHCs consist of battery-type electrodes, electrolyte, and capacitor-type electrodes. They are classified into two types: (1) capacitor-type cathodes (carbon materials or pseudocapacitive materials) *versus* battery-type anodes (metallic electrodes) and (2) battery-type cathodes (transition metal oxides) *versus* capacitor-type anodes (carbon materials or pseudocapacitive materials). The energy storage process in capacitive electrodes is associated with the adsorption/desorption or intercalation/de-intercalation of ions at the cathode or anode. The energy storage process in the battery-type electrode differs significantly. The former is due to metal ion deposition/stripping at anodes, whereas the latter is due to metal ion insertion/extraction at cathodes.

**3.2.1. Configuration of capacitor-type cathodes *versus* battery-type anodes.** The capacitor-type electrode is a critical

component of MIHCs, while the battery-type electrode has been shown to be usually made of metal. Typically, capacitor-type electrode materials are usually made of carbon and pseudocapacitive materials. Capacitor-type electrode materials have higher rate capability and cycling stability than battery-type electrode materials due to the adsorption/desorption (or intercalation/de-intercalation) of metal ions, but their specific capacitance is lower. The device's energy density is governed by the capacitor-type electrode materials, which are themselves determined by the short board effect. Therefore, the development of high-capacitance electrode materials has been a recent focus of research in the field of MIHCs, especially in ZHCs. As an important candidate for capacitor-type cathodes, carbon materials have always received great attention.

**3.2.2. Configuration of battery-type cathodes *versus* capacitor-type anodes.** For the configuration of battery-type cathodes *versus* capacitor-type anodes, the battery-type electrode is another critical component of MIHCs. Apart from metals, the majority of battery-type electrode materials are transition metal oxides, such as manganese- and vanadium-based oxides. Although battery-type electrode materials have a greater specific capacity than capacitor-type electrode materials owing to the deposition/stripping (or insertion/extraction) of metal ions, their rate capability and cycle performance are much lower. In other words, the materials used in battery-type electrodes dictate the device's power capability and cycle performance. As a result, it is critical to develop and commercialize high-rate, stable battery-type electrode materials for MIHCs. Table 2 summarizes current research on these battery-type cathode materials with corresponding carbon-material capacitor-type anodes in MIHCs. In recent years, the research on MIHCs has mainly focused on ZHCs, while the research results on Mg, Al, and Ca-based hybrid capacitors are fewer due to kinetic limitations, leading to the development of more electrode materials suitable for Zn-ion energy storage.

## 4. Carbon-based nanomaterials in MIHCs

Carbon materials occur in a variety of forms. Due to their high SSA, plentiful pores, chemical inertness, and good conductivity, porous carbon (PC), graphene, carbon aerogels (CAs), and carbon nanotubes (CNTs) are intriguing research topics for application in MIHCs. When carbon materials are reduced to the nanoscale, their characteristics significantly alter. The varying dimensions of the carbon nanostructure impart diverse qualities to carbon-based materials. As a result, this section will explore numerous carbon nanostructures with varying dimensions. The current classification of different carbon nanomaterials is shown in Fig. 5.

Currently, for carbon nanomaterials, effective ways to increase performance include doping, hybridization, surface modification and specific structure construction. The carbon-based nanomaterials used for different MIHCs and their performance with potentials intervals are shown in Table 3.



Table 2 Electrochemical performance of recently reported battery-type anodes with carbon materials as the capacitor-type cathode in MIHCs

| Electrode material                                | Electrolyte  | Voltage (V) | Energy density              | Power density             | Performance  | Application | Ref. |
|---|--|-------------|-----------------------------|---------------------------|--|-------------|------|
| Zn-doped $\delta$ -MnO <sub>2</sub>               | 2 M ZnSO <sub>4</sub>                                  | 0–2         | 157.2 W h kg <sup>-1</sup>  | 16 000 W kg <sup>-1</sup> | 80.2% after 30 000 cycles at 2 A g <sup>-1</sup>   | Zn-based    | 25   |
| AMX-Zn  | 2 M ZnSO <sub>4</sub>                                  | 0.3–1.9     | 60.2 W h kg <sup>-1</sup>   | 7.04 kW kg <sup>-1</sup>  | 92.5% after 10 000 cycles at 3.3 A g <sup>-1</sup> | Zn-based    | 26   |
| V <sub>2</sub> O <sub>5</sub>                     | 2 M ZnSO <sub>4</sub>                                  | –1 to 1.5   | 34.6 W h kg <sup>-1</sup>   | 1.3 kW kg <sup>-1</sup>   | 97.3% after 6000 cycles at 0.5 A g <sup>-1</sup>   | Zn-based    | 27   |
| V <sub>2</sub> O <sub>5</sub> -activated carbon   | 3 M Zn(CF <sub>3</sub> SO <sub>3</sub> ) <sub>2</sub>  | 0–2         | 53.13 W h kg <sup>-1</sup>  | 1384.6 W kg <sup>-1</sup> | ~99% after 4000 cycles at 0.1 mA cm <sup>-2</sup>  | Zn-based    | 28   |
| MnO <sub>2</sub> -CNTs                            | 2.69 M ZnSO <sub>4</sub> and 0.135 M MnSO <sub>4</sub> | 0–2         | 98.6 W h kg <sup>-1</sup>   | 2480.6 W kg <sup>-1</sup> | 83.6% after 15 000 cycles at 1 A g <sup>-1</sup>   | Zn-based    | 29   |
| PDA@3DVAG   | 2 M ZnSO <sub>4</sub>                                  | 0.5–2       | 46.14 W h kg <sup>-1</sup>  | 2183 W kg <sup>-1</sup>   | 61.8% after 3000 cycles at 1 A g <sup>-1</sup>     | Zn-based    | 30   |
| $\delta$ -MnO <sub>2</sub> @CAC                   | 2 M ZnSO <sub>4</sub>                                  | 0–1.9       | 90 W h kg <sup>-1</sup>     | 3838 W kg <sup>-1</sup>   | 80.7% after 16 000 cycles at 10 A g <sup>-1</sup>  | Zn-based    | 31   |
| V <sub>2</sub> CT <sub>x</sub>                    | 1 M LiSO <sub>4</sub>                                  | 0.1–1.85    | 386.2 W h kg <sup>-1</sup>  | —                         | 100% after 18 000 cycles at 10 A g <sup>-1</sup>   | Zn-based    | 32   |
| MnO <sub>2</sub> /graphite hybrids                | 2 M ZnSO <sub>4</sub> and 0.5 M MnSO <sub>4</sub>      | 0.8–1.8     | 247 W h kg <sup>-1</sup>    | 11.78 kW kg <sup>-1</sup> | 80.8% after 1000 cycles at 1 A g <sup>-1</sup>     | Zn-based    | 33   |
| K-MnO <sub>2</sub>                                | 1 M MgSO <sub>4</sub>                                  | 0–1.8       | 85.2 W h kg <sup>-1</sup>   | 360 W kg <sup>-1</sup>    | 96.7% after 20 000 cycles at 5 A g <sup>-1</sup>   | Mg-based    | 34   |
| E-MoS <sub>2</sub>                                | 1 M MgSO <sub>4</sub>                                  | 0–1.8       | 192.8 W h kg <sup>-1</sup>  | 1627 W kg <sup>-1</sup>   | 93.8% after 30 000 cycles at 5 A g <sup>-1</sup>   | Mg-based    | 35   |
| Al <sub>x</sub> MnO <sub>2-z</sub> /AC            | 0.5 M MgSO <sub>4</sub>                                | 0–2         | 104.86 W h kg <sup>-1</sup> | 69.44 W kg <sup>-1</sup>  | 86% after 2000 cycles at 1 A g <sup>-1</sup>       | Mg-based    | 36   |
| Mg-OMS-2/graphene                                 | 0.5 M Mg(NO <sub>3</sub> ) <sub>2</sub>                | 0–2         | 46.9 Wh kg <sup>-1</sup>    | 70 W kg <sup>-1</sup>     | 93% after 300 cycles at 0.1 A g <sup>-1</sup>      | Mg-based    | 37   |
| Mg-OMS-2/graphene                                 | 0.5 M MgCl <sub>2</sub>                                | 0–2         | —                           | —                         | 75.7% after 300 cycles at 0.1 A g <sup>-1</sup>    | Mg-based    | 37   |
| Mg-OMS-2/graphene                                 | 0.5 M MgSO <sub>4</sub>                                | 0–2         | —                           | —                         | 57.5% after 300 cycles at 0.1 A g <sup>-1</sup>    | Mg-based    | 37   |
| RAT-Ti <sub>3</sub> C <sub>2</sub> T <sub>x</sub> | 1 M Al <sub>2</sub> (SO <sub>4</sub> ) <sub>3</sub>    | 0–2         | 112 W h L <sup>-1</sup>     | 30 000 W L <sup>-1</sup>  | 91.8% after 10 000 cycles at 5 A g <sup>-1</sup>   | Al-based    | 24   |
| CuFe-PBA  | 1 M Al(NO <sub>3</sub> ) <sub>3</sub>                  | 0–2         | 13 W h kg <sup>-1</sup>     | —                         | ~80% after 1000 cycles at 0.25 A g <sup>-1</sup>   | Al-based    | 38   |
| MCM/V <sub>2</sub> O <sub>5</sub>                 | 1 M Al <sub>2</sub> (SO <sub>4</sub> ) <sub>3</sub>    | 0–1.6       | 18.0 W h kg <sup>-1</sup>   | 147 W kg <sup>-1</sup>    | 88% after 10 000 cycles at 0.5 A g <sup>-1</sup>   | Al-based    | 39   |
| Sn  | Ca(PF <sub>6</sub> ) <sub>2</sub>                      | 1.5–4.8     | —                           | —                         | 84% after 1000 cycles at 0.2 A g <sup>-1</sup>     | Ca-based    | 23   |



Fig. 5 An overview of mainstream carbon material classification.

The research on carbon materials used in ZHCs dominates the development of carbon materials for MIHCs.

#### 4.1. Zero-dimensional carbon materials

The term “zero-dimensional (0-D) carbon materials” refers to sphere-shaped carbon materials with an aspect ratio of  $\sim 1$ . Activated carbon (AC), carbon quantum dots (CQD), nanodiamonds, and carbon nanospheres are the most common 0-D carbon materials. 0-D carbon materials usually show high SSAs (hundreds to thousands of m<sup>2</sup> g<sup>-1</sup>) and customizable pore size

and distribution, which are crucial parameters affecting the supercapacitor's performance.

0-D carbon materials are extensively employed as electrode materials, with electrons provided either by hopping between neighboring nanoparticles' trap states or *via* diffusive movement within the extended states, which is hindered by (de)trapping processes.<sup>68,69</sup> The absence of continuity between carbon nanoparticles is unfavorable for enhancing the electrical conductivity and, as a result, the power density reduces. Typically, 0-D carbon compounds are synthesized from carbon-rich precursors by thermal activation at high temperatures (700–1200 °C) with H<sub>2</sub>O, CO<sub>2</sub>, and air, or chemical activation at lower temperatures (600–800 °C) with H<sub>3</sub>PO<sub>4</sub>, KOH, ZnCl<sub>2</sub>, and others.<sup>70</sup> Previously published data indicate that activated carbon could show a specific capacitance of 100–300 F g<sup>-1</sup>.<sup>71–73</sup> Song *et al.* effectively prepared activated carbon cathode material for ZHCs by direct KOH activation utilizing pitch coke (PHC) and petroleum coke (PMC) as precursors.<sup>42</sup> The results exhibited excellent electrochemical performances with an exceptional specific capacitance of 146.4 mA h g<sup>-1</sup> at 0.1 A g<sup>-1</sup> after 5000 cycles.

0-D carbon nanospheres have a multitude of applications in MIHCs, where they may facilitate the conduction of cations in electrodes with an optimal pore size distribution. Chen *et al.* presented an electrode strategy for dual ion adsorption and manufactured nitrogen-doped mesoporous carbon nanospheres for ZHCs, as shown in Fig. 6.<sup>74</sup> The study illustrates the usage of nitrogen-doped mesoporous carbon nanospheres (NMCSs) with hierarchically distributed pores and improved Zn<sup>2+</sup> storage capacity. The as-prepared aqueous ZHCs had a notable specific capacity of 157.8 mA h g<sup>-1</sup>, a maximum energy density of 126.2 W h kg<sup>-1</sup> at 0.2 A g<sup>-1</sup>, and an ultra-high power density of 39.9 kW kg<sup>-1</sup> with a rapid charging time of 5.5 s.





Table 3 Recent advances in carbon-based electrodes for MIHCs

| Electrode material                | Electrolyte  | Voltage [V] | Energy density             | Power density              | Cycling stability                                       | Dimension | Application | Ref. |
|-----------------------------------|--|-------------|----------------------------|----------------------------|---|-----------|-------------|------|
| Commercial AC                     | 2 M ZnSO <sub>4</sub>  | 0.2–1.8     | 104.8 W h kg <sup>-1</sup> | 383.5 W kg <sup>-1</sup>   | 95.1% after 10 000 cycles at 4 A g <sup>-1</sup>        | 0-D       | Zn-based    | 40   |
| AC treated by gradient acid       | Glutaraldehyde crosslinked gelatin                           | 0.2–1.8     | —                          | —                          | 92.1% after 10 000 cycles at 1 A g <sup>-1</sup>        | 0-D       | Zn-based    | 41   |
| AC-PHC                            | 1 M ZnSO <sub>4</sub>  | 0.2–1.8     | 117 W h kg <sup>-1</sup>   | 160 W kg <sup>-1</sup>     | 95% after 5000 cycles at 5 A g <sup>-1</sup>            | 0-D       | Zn-based    | 42   |
| Mg-OMS-2/graphene                 | Mg(TFSI) <sub>2</sub> -Pyr <sub>14</sub> TFSI                | 0.6–2.0     | —                          | —                          | > 100% after 50 cycles at 50 mA g <sup>-1</sup>         | 0-D       | Mg-based    | 19   |
| Mg-OMS-2/graphene                 | 0.5 M Mg(NO <sub>3</sub> ) <sub>2</sub>                      | 0–2         | 46.9 W h kg <sup>-1</sup>  | 70 W kg <sup>-1</sup>      | 93% after 300 cycles at 0.1 A g <sup>-1</sup>           | 0-D       | Mg-based    | 37   |
| Mg-OMS-2/graphene                 | 0.5 M MgCl <sub>2</sub>                                      | 0–2         | —                          | —                          | 75.7% after 300 cycles at 0.1 A g <sup>-1</sup>         | 0-D       | Mg-based    | 37   |
| MEC                               | 0.5 M MgSO <sub>4</sub>                                      | 0–2         | —                          | —                          | 57.5% after 300 cycles at 0.1 A g <sup>-1</sup>         | 0-D       | Mg-based    | 43   |
| AC                                | 0.5 M Mg(TFSI) <sub>2</sub>                                  | –2 to 2     | 106 W h kg <sup>-1</sup>   | 11.87 kW kg <sup>-1</sup>  | > 90% after 10 000 cycles at 1 A g <sup>-1</sup>        | 0-D       | Mg-based    | 44   |
| AC                                | 0.5 M MgCl <sub>2</sub>                                      | –0.8 to 0.8 | 103.2 W h kg <sup>-1</sup> | 2 kW kg <sup>-1</sup>      | 92% after 20 000 cycles at 10 A g <sup>-1</sup>         | 0-D       | Mg-based    | 23   |
| MEC                               | CaI(PF <sub>6</sub> ) <sub>2</sub>                           | 1.5–4.8     | —                          | —                          | 84% after 1000 cycles at 0.2 A g <sup>-1</sup>          | 0-D       | Ca-based    | 43   |
| AC                                | 0.5 M Ca(TFSI) <sub>2</sub>                                  | –2 to 2     | —                          | —                          | —   | 0-D       | Ca-based    | 43   |
| AC                                | [EMIm]Cl & AlCl <sub>3</sub>                                 | 0–2         | 51 W h kg <sup>-1</sup>    | 9.285 kW kg <sup>-1</sup>  | 97.9% after 10 000 cycles at 5 A g <sup>-1</sup>        | 0-D       | Al-based    | 45   |
| MCM/N <sub>2</sub> O <sub>5</sub> | 1 M Al <sub>2</sub> (SO <sub>4</sub> ) <sub>3</sub>          | 0–1.6       | 18.0 W h kg <sup>-1</sup>  | 147 W kg <sup>-1</sup>     | 88% after 10 000 cycles at 0.5 A g <sup>-1</sup>        | 0-D       | Al-based    | 39   |
| NCN/carbon nanotube               | 2 M ZnSO <sub>4</sub>  | 0.2–1.6     | 124.1 W h kg <sup>-1</sup> | 34.7 W kg <sup>-1</sup>    | 100% after 1000 cycles at 1 A g <sup>-1</sup>           | 0-D + 1-D | Zn-based    | 46   |
| CNT/PANI                          | 2 M ZnSO <sub>4</sub>  | 0.5–1.5     | 104 W h kg <sup>-1</sup>   | 8.3 kW kg <sup>-1</sup>    | Nearly 100% after 1000 cycles at 1 A g <sup>-1</sup>    | 1-D       | Zn-based    | 47   |
| CNT/paper                         | 2 M ZnSO <sub>4</sub>  | 0.2–1.8     | —                          | —                          | Nearly 100% after 7000 cycles at 2 A g <sup>-1</sup>    | 1-D       | Zn-based    | 48   |
| CNT/paper                         | 2 M ZnSO <sub>4</sub>  | 0.2–1.8     | —                          | —                          | Nearly 100% after 7000 cycles at 2 A g <sup>-1</sup>    | 1-D       | Zn-based    | 48   |
| CNPK                              | 1 M ZnSO <sub>4</sub>  | 0–1.9       | 81.1 W h kg <sup>-1</sup>  | 13.366 kW kg <sup>-1</sup> | 101.8% after 10 000 cycles at 5 A g <sup>-1</sup>       | 2-D       | Zn-based    | 49   |
| NPCNs                             | 2 M ZnSO <sub>4</sub>  | 0–1.7       | 64.8 W h kg <sup>-1</sup>  | 1099 W kg <sup>-1</sup>    | Nearly 100% after 10 000 cycles at 5 A g <sup>-1</sup>  | 2-D       | Zn-based    | 50   |
| MCLNS                             | 1 M ZnSO <sub>4</sub>  | 0.2–1.8     | 102.1 W h kg <sup>-1</sup> | 16.9 kW kg <sup>-1</sup>   | 98.7% after 10 000 cycles at 20 A g <sup>-1</sup>       | 2-D       | Zn-based    | 51   |
| OPCNF-20                          | 1 M ZnSO <sub>4</sub>  | 0–3.6       | 97.7 W h kg <sup>-1</sup>  | 9.9 kW kg <sup>-1</sup>    | 81% after 50 000 cycles at 1 A g <sup>-1</sup>          | 2-D       | Zn-based    | 52   |
| rGO + B90/FTO                     | 2 M ZnSO <sub>4</sub>  | 0.2–1       | 668 mW h kg <sup>-1</sup>  | 16 250 mW kg <sup>-1</sup> | ~90% after 1000 cycles at 20 mA g <sup>-1</sup>         | 2-D       | Zn-based    | 53   |
| <i>In situ</i> pillared Mxene     | 0.1 M ZnSO <sub>4</sub>                                      | 0.01–1      | —                          | —                          | Over 96% after 1000 cycles at 0.2 A g <sup>-1</sup>     | 2-D       | Zn-based    | 54   |
| Graphene                          | 2 M ZnSO <sub>4</sub>  | 0.1–1.9     | 78.32 W h kg <sup>-1</sup> | 8010 W kg <sup>-1</sup>    | 90.8% after 10 000 cycles at 1 A g <sup>-1</sup>        | 2-D       | Zn-based    | 55   |
| WC-6ZnN-12U                       | 1 M ZnSO <sub>4</sub>  | 0.2–1.8     | 109.5 W h kg <sup>-1</sup> | 225 W kg <sup>-1</sup>     | 92.7% after 50 000 cycles at 2 A g <sup>-1</sup>        | 2-D       | Zn-based    | 56   |
| PPy/N-rGO                         | 2 M ZnSO <sub>4</sub>  | 0–1.6       | 232.5 W h kg <sup>-1</sup> | 160 W kg <sup>-1</sup>     | 85% after 10 000 cycles at 7 A g <sup>-1</sup>          | 2-D       | Zn-based    | 57   |
| Graphene                          | 6% KI & MgSO <sub>4</sub>                                    | 0–1.3       | 69.3 W h kg <sup>-1</sup>  | 2.5 kW kg <sup>-1</sup>    | 89% after 5000 cycles at 5 A g <sup>-1</sup>            | 2-D       | Mg-based    | 58   |
| AC                                | Mg(TFSI) <sub>2</sub> -Pyr <sub>14</sub> TFSI                | 0.6–2.0     | —                          | —                          | > 100% after 50 cycles at 50 mA g <sup>-1</sup>         | 2-D       | Mg-based    | 19   |
| RHOPC                             | 1 M Al <sub>2</sub> (SO <sub>4</sub> ) <sub>3</sub>          | 0–2         | 112 W h L <sup>-1</sup>    | 30 000 W L <sup>-1</sup>   | 91.8% after 10 000 cycles at 5 A g <sup>-1</sup>        | 0-D       | Al-based    | 24   |
| 3D porous carbon                  | Glutaraldehyde crosslinked gelatin/ZnSO <sub>4</sub>         | 0.2–1.8     | 82.36 W h kg <sup>-1</sup> | 3760 W kg <sup>-1</sup>    | 87.6% after 10 000 cycles at 1 A g <sup>-1</sup>        | 3-D       | Zn-based    | 59   |
| ACTS-800                          | 3 M ZnSO <sub>4</sub>  | 0–2         | 127 W h kg <sup>-1</sup>   | 7920 W kg <sup>-1</sup>    | 100% after 1000 cycles at 10 A g <sup>-1</sup>          | 3-D       | Zn-based    | 60   |
| HHPC6                             | 2 M ZnSO <sub>4</sub>  | 0.2–1.8     | 117.6 W h kg <sup>-1</sup> | 40 kW kg <sup>-1</sup>     | 88% after 20 000 cycles at 5 A g <sup>-1</sup>          | 3-D       | Zn-based    | 61   |
| PZC-A750                          | 1 M Zn(CF <sub>3</sub> SO <sub>3</sub> ) <sub>2</sub>        | 0.2–1.8     | 107.3 W h kg <sup>-1</sup> | 24.9 kW kg <sup>-1</sup>   | Nearly 100% after 10 000 cycles at 10 A g <sup>-1</sup> | 3-D       | Zn-based    | 62   |
| MOF derived carbon (MDC)          | 1 M ZnSO <sub>4</sub>  | 0.1–1.7     | 7.5 W h kg <sup>-1</sup>   | 85.5 kW kg <sup>-1</sup>   | 99% after 20 000 cycles at 1 A g <sup>-1</sup>          | 3-D       | Zn-based    | 63   |
| BSCs                              | 1 M ZnSO <sub>4</sub>  | 0–1.0       | 197.7 W h kg <sup>-1</sup> | 15.221 kW kg <sup>-1</sup> | 106.1% after 10 000 cycles at 0.1 A g <sup>-1</sup>     | 3-D       | Zn-based    | 64   |
| CDC                               | 2 M ZnSO <sub>4</sub>  | 0–2.0       | 243 W h kg <sup>-1</sup>   | 492 W kg <sup>-1</sup>     | 85% after 20 000 cycles at 0.5 A g <sup>-1</sup>        | 3-D       | Zn-based    | 65   |
| 3D printed rGO                    | 1 M ZnSO <sub>4</sub>  | 0.01–1.8    | 266 μW h cm <sup>-2</sup>  | ~100 μW cm <sup>-2</sup>   | 75% after 10 000 cycles at 10 A g <sup>-1</sup>         | 3-D       | Zn-based    | 66   |
| 3D AC                             | Zn(BF <sub>4</sub> ) <sub>2</sub> with [EMIN]BF <sub>4</sub> | –0.7 to 2.4 | 220 W h kg <sup>-1</sup>   | 9.5 kW kg <sup>-1</sup>    | 95% after 20 000 cycles at 2 A g <sup>-1</sup>          | 3-D       | Zn-based    | 67   |



Fig. 6 (a) Schematic illustration of the fabrication of NMCSs. SEM images of (b)  $\text{SiO}_2@/\text{SiO}_2/\text{C}$  and (c) NMCSs. (d and e) TEM and (f) high-resolution (g) HAADF-STEM image and elemental mappings of NMCSs.<sup>74</sup> Reused with permission from Springer Nature.

## 4.2. One-dimensional carbon materials

One-dimensional (1-D) carbon materials are attractive candidates for MIHCs electrodes owing to their lengthy 1-D nanostructure, which facilitates the formation of a sequential network for charge transfer.<sup>75</sup>

**4.2.1. Carbon nanotubes.** Carbon nanotubes (CNTs) are one of the most common kinds of 1-D carbon material. They have garnered considerable interest since their discovery and have far greater electrical conductivity than AC. CNTs are classified as single- or multi-walled carbon nanotubes (SWCNTs or MWCNTs). Usually, they can be synthesized using arc discharge, pulsed laser vaporization, high pressure carbon monoxide disproportionation and chemical vapor deposition (CVD).<sup>76–78</sup> The microdistribution of CNTs significantly affected the electrochemical properties, and the aligned CNTs have better electronic conductivity than the entangled CNTs.<sup>79</sup> Pure carbon nanotubes were previously reported to have a specific capacitance in the range of 20–100  $\text{F g}^{-1}$  in an aqueous electrolyte.<sup>80–82</sup> However, the capacitance of CNTs is restricted due to the hydrophobic feature and the small SSA. The specific capacitance of carbon nanotubes remains approximately 150  $\text{F g}^{-1}$  when treated with acid.<sup>83</sup>

Aqueous ZHCs have been widely explored in the literature. Dong *et al.* have indicated that functionalized carbon nanotubes outperform pristine CNTs in terms of electrochemical performance taking advantage of better chemical adsorption ability and hydrophilicity of  $\text{Zn}^{2+}$ , and the functionalized carbon nanotube (f-CNT)/polyaniline (PANI) nanocomposites successfully integrated capacitive energy storage mechanism of



Fig. 7 SEM images of (a) pure PANI and (b) h-CNT/PANI nanomaterial. (c) TEM image of h-CNT/PANI nanomaterial. (d) XRD patterns of h-CNTs, pure PANI and h-CNT/PANI nanomaterial.<sup>47</sup> Reused with permission from Elsevier.

f-CNTs with the redox reaction energy storage mechanism of PANI, therefore exhibiting better comprehensive electrochemical properties, such as good rate performance, high capacity, and long cycle life.<sup>47</sup> In addition, with the prepared nanomaterial, flexible and high-performance zinc-based devices have been generated. Micromorphologies of pure PANI and hydroxylated carbon nanotube (h-CNT)/PANI nanocomposites are shown in Fig. 7a–c.<sup>47</sup> Pure PANI samples generated by oxidation polymerization were nanorods with a diameter of less than 50 nm. In h-CNT/PANI nanocomposites, the particles



showed similar nanorod-like morphology, albeit their width and length were much reduced. The TEM in Fig. 7c demonstrates the PANI coating on the surface of h-CNTs in the h-CNT/PANI nanocomposite. In such a situation, electrons may travel *via* highly conductive h-CNTs to PANI, hence facilitating PANI's involvement in redox processes. The presence of h-CNT contributes to the enhancement of PANI's hydrophilicity.

**4.2.1. Carbon nanofibers.** Carbon nanofibers (CNFs) are another intriguing 1-D carbon material for flexible electrodes that may be synthesized using CVD or *via* simple electrospinning technologies.<sup>84–86</sup> Appropriate pore size and distribution are important factors for the application of CNFs in energy storage. The low energy density of CNFs limits their utility in MIHCs because of the lack of active sites. Recently, Zhang *et al.* proposed a carbon nanofiber-based flexible electrode with numerous adsorption sites.<sup>87</sup> The study describes an *in situ* exfoliation technique for modifying the chemisorption sites of carbon nanofibers by means of high pyridine/pyrrole nitrogen doping and carbonyl functionalization. The highly electronegative pyridine/pyrrole nitrogen dopants can not only lower the binding energy between carbonyl groups and Zn<sup>2+</sup> by causing the charge delocalization of carbonyl groups, but they can also increase the adsorption of Zn<sup>2+</sup> by interacting with carbonyl groups. The resulting carbon nanofiber thin film cathode exhibited a high energy density of 98.28 W h kg<sup>-1</sup> at a power density of 72.27 W kg<sup>-1</sup> and an ultra-long lifetime with a capacity retention of 99.2% after 200 000 cycles at 40 A g<sup>-1</sup> under the condition of high loading (14.45 mg cm<sup>-2</sup>).

### 4.3. Two-dimensional carbon materials

Two-dimensional (2-D) carbon materials, such as graphene, have garnered significant interest for their use in hybrid capacitor electrodes due to several unique properties. First of all, 2-D carbon materials possess high mechanical stability and flexibility, making them ideal for use in flexible electronic devices and energy storage systems. The mechanical stability of 2-D carbon materials enables them to withstand the repeated charge–discharge cycles and electrochemical reactions that occur in hybrid capacitors, while their flexibility makes them well-suited for use in flexible and bendable electronics. On the other hand, 2-D carbon materials have high electrical conductivity and thermal conductivity, making them ideal for use as electrodes in hybrid capacitors. The high electrical conductivity enables fast and efficient flow of charge in the capacitor, reducing the internal resistance and improving the power density of the device. The high thermal conductivity helps to dissipate heat during high-power operation, reducing the risk of thermal damage to the device. In addition, 2-D carbon materials have a high surface area and chemical stability, making them highly resistant to degradation in aqueous and non-aqueous electrolytes. The high surface area provides ample room for electrochemical reactions to occur, resulting in a higher capacitance compared to that of traditional 3-D electrodes. The chemical stability of 2-D carbon materials helps to extend the life of the capacitor, increasing its reliability and durability.

**4.3.1. Graphene.** Graphene is a typical 2-D carbon material that consists of a one-atom-thick monolayer of sp<sup>2</sup>-hybridized carbon. It is a zero-band gap semi-metallic material with a Dirac cone-like energy band structure near the Fermi plane, resulting in a very high room-temperature carrier mobility (15 000 cm<sup>2</sup> V<sup>-1</sup> s<sup>-1</sup>). Graphene possesses a number of inherent chemical and physical properties, including high mechanical strength (1 TPa), excellent mass and heat transfer capability, extremely high light transmittance (97%), and a large SSA (2675 m<sup>2</sup> g<sup>-1</sup>).

Recently, Dou *et al.* have found that it is currently challenging to create cathode materials that are compatible with Zn-ion hybrid capacitors due to the poor knowledge of charge storage behavior,<sup>88</sup> as shown in Fig. 8. However, the bulk of previous research has concentrated on understanding the influence of oxygen-containing groups without taking the graphitic structure into account. The surface properties of reduced graphene oxide (rGO) nanosheets are used to optimize their charge storage capacity and electrochemical kinetics. In addition to the contribution of oxygen-containing groups, the reversible adsorption/desorption of H<sup>+</sup> on carbon atoms of rGO sheets has been shown to contribute. Electrochemical studies and density functional theory calculations show that H<sup>+</sup> causes cloud rupture in the aromatic domain, as well as graphitic structural distortion/restoration and C sp<sup>2</sup>–sp<sup>3</sup> re-hybridization. The rGO thermally treated at 200 °C achieves the optimum electrochemical performance with a specific capacitance of 245 F g<sup>-1</sup> at 0.5 A g<sup>-1</sup> and a retention of 53% at 20 A g<sup>-1</sup>. The mentioned study has pushed the frontiers of proton adsorption chemistry and provided additional information on the development of novel electrode materials.

**4.3.2. Graphdiyne.** Graphdiyne (GDY) is a novel class of 2-D carbon materials generated by the joining of sp and sp<sup>2</sup> hybridized carbon, as shown in Fig. 9.<sup>89</sup> Due to the presence of sp hybridized carbon, graphene has a structure that is fundamentally different from that of conventional carbon materials, resulting in distinct characteristics. For example, sp and sp<sup>2</sup> hybridized carbons allow GDY to have a higher chemical activity while maintaining stable physical features. The activity of the C≡C bond may enhance the chemical characteristics of carbon compounds when stimulated externally (light, magnet, and electricity).

Additionally, enriched-conjugated systems exhibit excellent theoretical conductivity and charge transfer rates. Due to these qualities, GDY has the potential to significantly enhance the manufacture of high-performance electrical products. The processes used to synthesize GDY are classified as dry or wet methods.<sup>90–92</sup> Li *et al.* utilized a 2D all-carbon GDY with superior 2D strength and strong mixed conductivities for both electrons and ions to shield multidimensional nickel cobalt oxide nanostructures and got an electrode for hybrid supercapacitors. The *in situ* formed GDY forms 3D interpenetrating networks with nanostructures, resulting in a considerable increase in conductivity and prevention of structural deterioration. The built hybrid asymmetric supercapacitor exhibited an excellent capacitance of 200.9 F g<sup>-1</sup> at 1 A g<sup>-1</sup>, with an energy density of



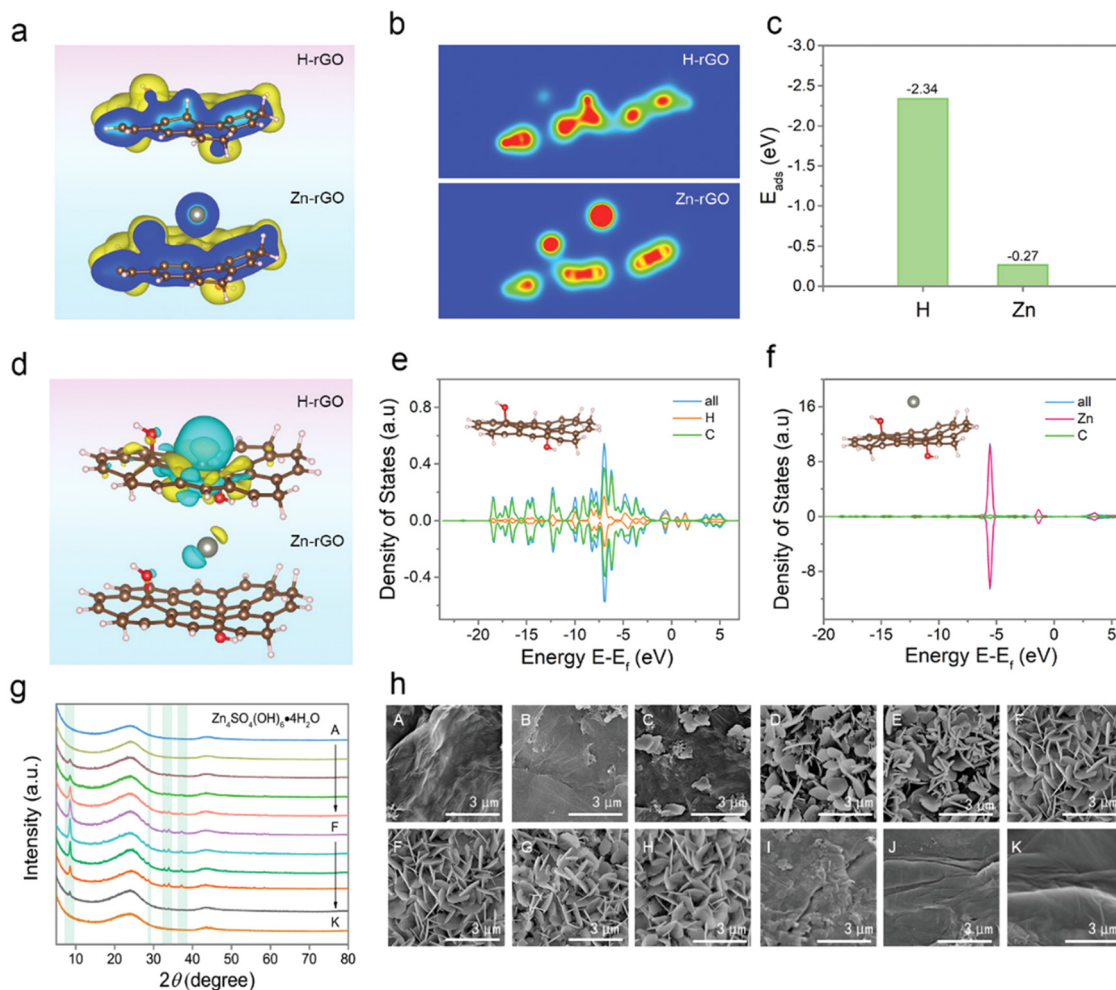


Fig. 8 (a) Structural energy, (b) charge distribution and (c) calculated adsorption energy, (d) optimized charge-density-difference patterns, and (e and f) density of the states of rGO with the H<sup>+</sup> and Zn<sup>2+</sup> adsorption.<sup>88</sup> Reused with permission from Wiley.

62.8 W h kg<sup>-1</sup> and a power density of 747.9 W kg<sup>-1</sup>. In a long-term 10 000-cycle test at a current density of 20 A g<sup>-1</sup>, the capacity retention can reach 97.7%.

#### 4.4. Three-dimensional carbon materials

Increased dimensionality means that a greater proportion of the active surface is in contact with the electrolyte, which significantly improves the electrochemical characteristics of electrode materials.<sup>93</sup> A three-dimensional (3-D) structure with well-connected holes, from this vantage point, not only provides continuous channels for optimal electrolyte contact, but also speeds up the charge transfer by minimizing diffusion paths.<sup>94</sup> 3-D carbon materials garnered significant interest for their use in hybrid capacitors due to several unique properties. First, 3-D carbon materials possess high surface area and conductivity, making them ideal for use as electrodes. The high surface area provides ample room for electrochemical reactions to occur, resulting in a higher capacitance compared to 2-D electrodes. The high conductivity of 3-D carbon materials ensures that the flow of charge is fast and efficient, reducing the internal resistance and improving the power density of the

hybrid capacitors. Second, 3-D carbon materials are flexible and lightweight, making them suitable for use in energy storage systems. Their mechanical stability and durability also make them ideal for use in demanding applications where high-performance energy storage is required. Third, 3-D carbon materials have a high chemical stability and corrosion resistance, making them highly resistant to degradation in aqueous and non-aqueous electrolytes. This property is particularly important in hybrid capacitors, where the electrode materials are subjected to repeated charge-discharge cycles and electrochemical reactions. The high chemical stability of 3-D carbon materials helps to extend the life of the capacitor, increasing its reliability and durability. Fourth, 3-D carbon materials are environmentally friendly, as they are made from renewable resources and do not contain harmful or toxic chemicals. This property makes them suitable for use in environmentally sensitive applications, such as in the automotive and aerospace industries, where the use of hazardous materials is strictly regulated.

Typically, 3-D carbon materials are generated using CVD, hydrothermal, or template methods. Due to sustainable





Fig. 9 Chemical structures and nomenclature. (a) Structure schematics of graphene and graphynes. (b)  $\alpha$ -graphyne; (c)  $\beta$ -graphyne; (d)  $\gamma$ -graphyne; (e) 6,6,12-graphyne; (f)  $\beta$ -graphdiyne; and (g) GDY.<sup>89</sup> Reused with permission from Royal Society of Chemistry.

development requirements, researchers have adopted some bio-residue-derived biochars for 3-D carbon material construction. Milica *et al.* suggested using a porous activated carbon produced from biochar to obtain Al-ion supercapacitors. As shown in Fig. 10, carbonized vine shoots (VS) were tested as electrode material for supercapacitors with aqueous electrolyte. Biochar prepared by pre-carbonization of VS (at 300 °C) was impregnated with ZnCl<sub>2</sub> at 600–700 °C to produce carbon with large micropore and mesopore volumes and a large SSA of close to 1500 m<sup>2</sup> g<sup>-1</sup>. A high specific capacitance was achieved in an Al-based electrolyte, allowing a working voltage of 1.8 V and delivering an energy density of 24 W h kg<sup>-1</sup> at 1 A g<sup>-1</sup>.<sup>95</sup>

#### 4.5. Carbon-based cathode design

The mechanism of adsorption/desorption or embedding/de-embedding of multivalent metal cations on carbon-based electrodes relies on the study of the solvation properties of various metals, mostly thought to correspond to the ion diameter. Understanding the solvation environment of each metal cation system and the energy required for desolvation may facilitate the study of carbon-based cathodes. Multivalent cations have a high charge density and strong interaction with the electrolyte and cathode material, making dissociation and solid-state diffusion kinetically unfavorable, which is one of the biggest challenges in developing multivalent metal cation batteries and other energy storage devices.<sup>96</sup> Typically, researchers look to low current densities and high temperatures to promote the embedding of metal cations, but under these conditions, side reactions tend to contribute more to capacity and are detrimental

to cycling stability. In recent studies, proton embedding has been the dominant reaction in many multivalent cationic energy storage devices, largely due to the aqueous electrolyte being employed.<sup>97</sup> In fact, however, protons can still be generated by solvent decomposition even in anhydrous systems. Cathode design usually takes the storage of solvated molecules or complex ions (*e.g.*, MgCl<sup>+</sup>, AlCl<sub>4</sub><sup>-</sup>, *etc.* in chlorine-containing systems) into consideration rather than the bare metal cations after stripping.<sup>96</sup> For example, much of the work in ZHC research has focused on studying aqueous solutions, such as ZnSO<sub>4</sub> or Zn(CF<sub>3</sub>SO<sub>4</sub>)<sub>2</sub>, as electrolyte systems. The presence of zinc salts in the electrolyte system inevitably produces zinc ions and solvated Zn([Zn(H<sub>2</sub>O)<sub>6</sub>]<sup>2+</sup>) ions. Their diameters differ greatly between 1.48 and 8.60 Å, respectively, and this increased size limits their embedding in the micro-pores of the carbon material, thus limiting the capacity.<sup>98</sup>

The weak bonding of multivalent metal cations to the surface of the carbon material is also a limitation for the capacity of MIHCs, especially for Mg<sup>2+</sup>. William *et al.* illustrated through the energy band structure that when Mg<sup>2+</sup> are adsorbed onto graphene, the Fermi energy level remains at the Dirac point and thus no charge transfer occurs.<sup>99</sup> Adjusting the layer spacing of the carbon material to adjust the Fermi energy level is a possible strategy, which can be inspired by the design of monovalent cationic capacitors.<sup>100</sup> These challenges and realities have led researchers to focus on the design of cathode structures. It has been shown that the insertion of surface functional groups, heteroatom doping, and the introduction of surface defects are key methods for enhancing the electrochemical



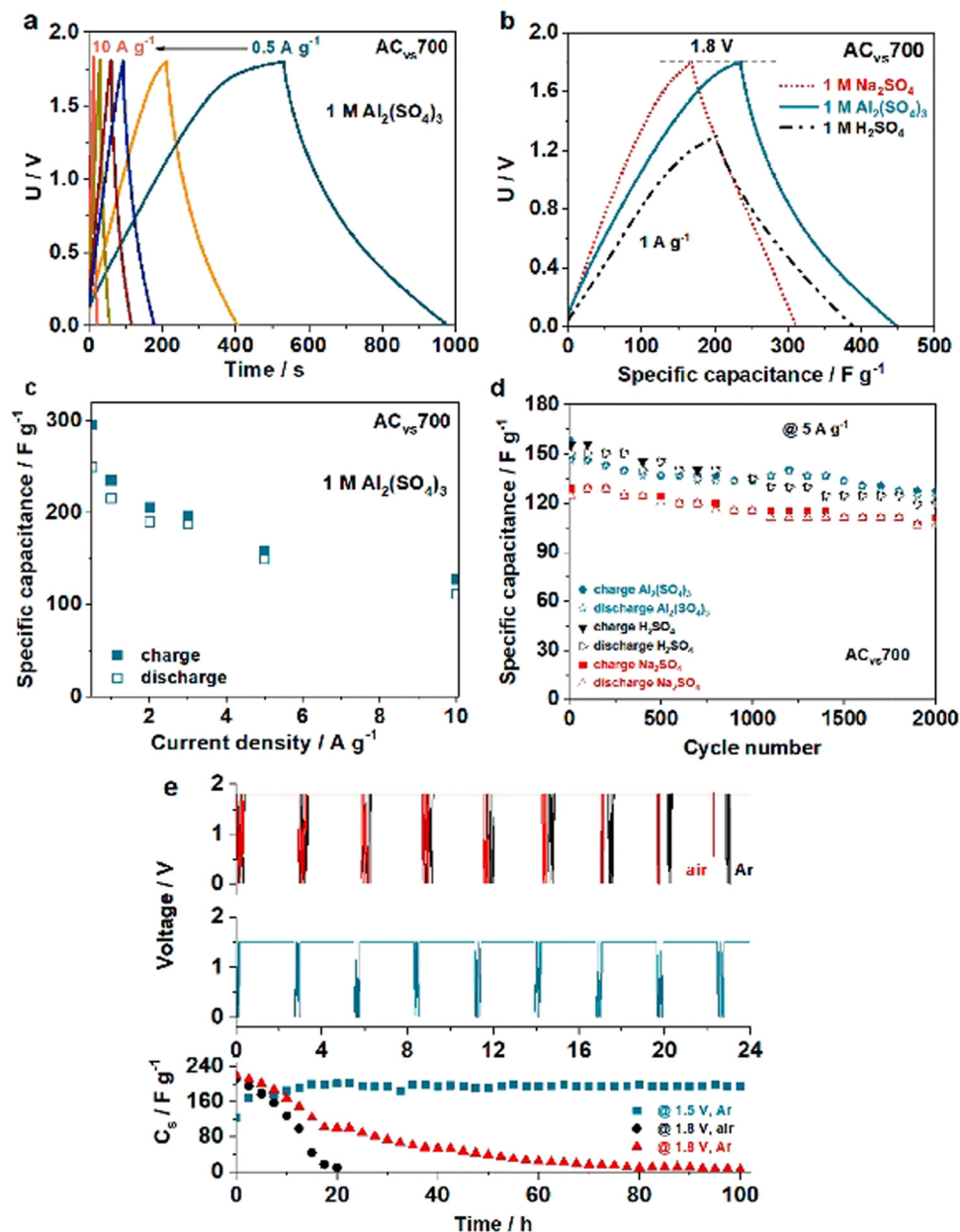


Fig. 10 (a) Charge/discharge curves at different current rates of  $\text{Al}_2(\text{SO}_4)_3$  electrolyte in a VS-based capacitor. (b)  $\text{Na}_2\text{SO}_4$  and  $\text{H}_2\text{SO}_4$  as comparison. (c) Specific capacitance, (d) number of cycles (e) floating test at 1.8 V of  $\text{Al}_2(\text{SO}_4)_3$  electrolyte in a VS-based capacitor in comparison with  $\text{Na}_2\text{SO}_4$  and  $\text{H}_2\text{SO}_4$ .<sup>95</sup> Reused with permission from Elsevier.

characteristics of carbon-based materials. Moreover, researchers have expended effort in optimizing the SSA and pore size distribution of carbon-based electrode materials. Nevertheless, the link between the pore characteristics of carbon materials and their energy storage capacity is ambiguous and needs further experimental and theoretical support.

The physical adsorption/desorption of ions on the surface of carbon materials is thought to be strongly influenced by the SSA. Kang *et al.* found that when activated carbon particles with an SSA of  $142 \text{ m}^{-2} \text{ g}^{-1}$  were used as a cathode, the discharge capacity of the assembled ZHCs was only  $9 \text{ mA h g}^{-1}$  at a current density of  $0.1 \text{ A g}^{-1}$ ; when a carbon black particle with a

higher SSA of  $1408 \text{ m}^{-2} \text{ g}^{-1}$  was used as the cathode material, it achieved a discharge capacity of  $78 \text{ mA h g}^{-1}$  at  $0.1 \text{ A g}^{-1}$ .<sup>101</sup> Notably, the cathode is involved in a series of side reactions in addition to the physical adsorption/desorption of cations. In the case of ZHCs, for example, the deposition/dissolution of  $\text{Zn}_4\text{SO}_4(\text{OH})_6 \cdot 5\text{H}_2\text{O}$  is involved in the cathode reaction. This deposition/dissolution process is irreversible and may lead to a rise in pH throughout the charge/discharge cycle of the ZHC, resulting in the creation of zinc oxide and the development of undesirable Zn dendrites.

Some researchers have argued that the SSA is not the only factor that affects MIHCs capacity. First, not all micropores on



the electrode material are accessible to the electrolyte ions. A cathode material design that considers both a suitable pore size distribution and a high specific surface area is an effective strategy to increase the capacity of MIHCs. An ideal pore structure should have a hierarchical structure with macropores (> 50 nm) for electrolyte penetration, mesopores (2–50 nm) for ion transport, and micropores (2 nm) for charge storage.<sup>102</sup> Ion migration in micropores is proportional to the size of the solvated molecules and the diameter of the pore.<sup>103</sup> In other words, ions have trouble crossing the energy barrier and entering pores when the size of the solvent molecules and solvated ions is larger than the size of the pores. Thus, although increasing the number of micropores increases the SSA, this is not necessarily accompanied by an increase in capacitance. Due to their pore size, mesoporous materials facilitate the fast transport of ions, hence improving electrochemical characteristics.<sup>104</sup> Additionally, a porous structure with a restricted distribution might shorten the ion transit length, improving the electrode kinetics.<sup>105</sup>

## 5. Conclusion and outlook

Compared to conventional metal ion batteries and supercapacitors, MIHCs offer high energy density and high-power density, ultra-long cycle life, safety, and more available polyvalent metal resources, making them very competitive for use in the energy storage industry. To fulfill the urgent need for high-performance energy storage and conversion, it is desired to develop innovative electrode materials for MIHCs. In particular, cathode development remains a major general challenge. As the multivalent metal cation energy storage technologies of interest have covered zinc, magnesium, calcium, aluminum, *etc.*, new members will be validated by drawing on the test procedures of mature energy storage technologies, such as monovalent ion supercapacitors, *etc.* It is worth noting that various research groups have invested efforts in improving the overall performance of MIHCs with the help of carbon nanomaterials of different dimensions (0, 1, 2, and 3) and asymmetrically designed pseudocapacitive materials, which has improved the specific capacitance of MIHCs devices. In this review, we comprehensively summarise the recent progress of multivalent cation hybrid capacitors and carbon-based electrodes, and from the existing representative results and comparisons, we draw the challenges that still need to be solved and the scope of future work.

(1) More battery-type electrode active materials should be developed, especially “beyond metal” type electrodes, and their reaction mechanisms should be studied in more detail. Due to the constraint of electrode materials, the majority of studies focus on ZHCs, whereas MHCs, CHCs, and AHCs get relatively little attention. The “beyond metal” material is crucial to the development of the anodes for these three hybrid capacitors, allowing for more stable cycling and increased efficiency. The future development of MIHCs anodes will focus on making them lightweight, highly stable, and cost-efficient. Moreover,

the electrochemical reaction mechanism of multivalent cations in MIHCs electrodes remains obscure. In contrast to monovalent cations, the ionic diameter, charge number, reactivity, ionic diffusion coefficient, and binding energy between ions and active materials of multivalent cations result in a distinct insertion–extraction kinetic energy storage mechanism in battery-type electrodes. The complexity of energy storage research is increasing. Other energy storage processes should exist in battery-type electrodes of MIHCs than ion adsorption/desorption, necessitating the adoption of more efficient and improved material characterization methodologies and electrochemical tests. With the advancement of technology, *in situ* infrared spectroscopy, *in situ* X-ray diffraction, and X-ray photoelectron spectroscopy may be used to monitor the surface groups, phases, and chemical states of electrodes in different charge–discharge states.

(2) Optimizing the structure of carbon-based electrode materials is an area that needs further attention. The cycling behaviour and power density of electrodes for all pseudocapacitive energy storage techniques must be enhanced since their performance is limited by the slow redox kinetics associated with intrinsic ion/electron transport. It is necessary to expand the potential window of carbon-based electrode materials in order to increase their working potential and energy density. Controlling the porosity of carbon-based materials is another crucial area of study. The optimal pore shape and size, as well as the relationship between carbonization precursors and carbonization procedures should be examined, in order to discover the optimum kinetics of carbon-based materials in the cycling behaviour of MIHCs. 3-D carbon compounds are structurally more appropriate for use as electrodes. Considering the recent research progress and the properties of carbon materials, the 3-D structure is more suitable for MIHC energy storage than 0-D, 1-D, and 2-D.

(3) Developing ecologically responsible, low-cost, and energy-efficient industrial manufacturing techniques for carbon nanomaterials. One obstacle preventing the industrialization of carbon-based materials is the high cost and high energy consumption of the carbonization and activation process. Therefore, it is vital to establish new manufacturing methods that are more streamlined. Notably, despite the fact that fine carbon material structures have been validated in the laboratory and have shown outstanding electrochemical performance, obstacles still exist in the synthesis of carbon nanomaterials on an industrial scale. Due to the mismatch between industrial test standards and laboratory test standards, a gap arises between scientific study and practical application that can only be bridged by the adoption of unified test standards. Understanding the compatibility of carbon materials with the development of electrode coating processes is essential, and special configurations of MIHCs can be achieved using screen printing, 3-D printing and other methods.

(4) The commercialization of carbon materials for use in MIHCs has been driven by the growing demand for high-power energy storage devices in a variety of industries, including consumer electronics, renewable energy, and electric vehicles.



In recent years, the production of carbon-based materials for hybrid capacitors has become more industrialized, with companies investing in large-scale production facilities and expanding their product offerings to meet the growing demand. Various energy storage technologies using metal cations as charge carriers are at different industrial stages. Japanese companies have successfully applied lithium-ion energy storage, sodium-ion energy storage and magnesium-ion energy storage technologies to industrial production, while Chinese companies are making efforts to commercialize sodium-ion energy storage technologies to a higher degree and the market size of sodium-ion energy storage is predicted to be over USD 6 billion in China by 2025. Dutch companies' mastery of aluminum ion energy storage technology is impressive, while calcium ion energy storage technology has been the slowest to develop in recent years. In the future, the commercialization of energy storage technology should be the focus of the development of enterprises in various countries. Despite the rapid growth and industrialization of carbon materials in hybrid capacitors, there are still some challenges that must be overcome to fully realize the potential of these materials. These include issues related to increasing mass loading in electrodes, scaling up production, improving performance, and reducing cost. Nevertheless, the continuous development and commercialization of carbon materials for hybrid capacitors has the potential to be greatly improved in the next decade.

## Author contributions

X. G. and G. H. conceived the project; C. J. C., I. P. P. and G. H. supervised the students; and all authors contributed to writing and revising the manuscript.

## Conflicts of interest

There are no conflicts to declare.

## Acknowledgements

The work was supported by Dean's prize-China Scholarship Council and Engineering and Physical Sciences Research Council (EPSRC; EP/V027433/1; EP/Y008707/1 and EP/V027433/2).

## References

- W. Zhang, Y. Wu, Z. Xu, H. Li, M. Xu, J. Li, Y. Dai, W. Zong, R. Chen and L. He, *Adv. Energy Mater.*, 2022, **12**, 2201065.
- W. Zuo, R. Li, C. Zhou, Y. Li, J. Xia and J. Liu, *Adv. Sci.*, 2017, **4**, 1600539.
- G. Z. Chen, *Int. Mater. Rev.*, 2017, **62**, 173–202.
- A. Riaz, M. R. Sarker, M. H. M. Saad and R. Mohamed, *Sensors*, 2021, **21**, 5041.
- X. Gao, X. Sun, J. Liu, N. Gao and H. Li, *J. Energy Storage*, 2019, **25**, 100901.
- X. Sun, J. Gao, C. Wang, X. Gao, J. Liu, N. Gao, H. Li, Y. Wang and K. Yu, *J. Chem. Eng.*, 2020, **383**, 123198.
- R. Chen, H. Ling, Q. Huang, Y. Yang and X. Wang, *Small*, 2022, **18**, 2106356.
- H. Xu and M. Shen, *Int. J. Energy Res.*, 2021, **45**, 20524–20544.
- R. Thangavel, B. Moorthy, D. K. Kim and Y. S. Lee, *Adv. Energy Mater.*, 2017, **7**, 1602654.
- H. Li, W. Zhang, K. Sun, J. Guo, K. Yuan, J. Fu, T. Zhang, X. Zhang, H. Long and Z. Zhang, *Adv. Energy Mater.*, 2021, **11**, 2100867.
- S. Nagamuthu, Y. Zhang, Y. Xu, J. Sun, F. Uz Zaman, D. K. Denis, L. Hou and C. Yuan, *J. Mater. Chem. A*, 2021, **10**, 357–378.
- A. D. Jagadale, R. C. Rohit, S. K. Shinde and D. Y. Kim, *ChemNanoMat*, 2021, **7**, 1082–1098.
- S. J. Patil, N. R. Chodankar, S.-K. Hwang, G. S. R. Raju, K. S. Ranjith, Y. S. Huh and Y.-K. Han, *Energy Storage Mater.*, 2022, **45**, 1040–1051.
- X. Gao, C. Zhang, Y. Dai, S. Zhao, X. Hu, F. Zhao, W. Zhang, R. Chen, W. Zong and Z. Du, *Small Struct.*, 2022, 2200316.
- X. Gao, X. Sun, Z. Jiang, Q. Wang, N. Gao, H. Li, H. Zhang, K. Yu and C. Su, *New J. Chem.*, 2019, **43**, 3907–3912.
- L. Han, J. Li, X. Zhang, H. Huang, Z. Yang, G. Zhu, M. Xu and L. Pan, *ACS Sustainable Chem. Eng.*, 2021, **9**, 9165–9176.
- S. Wu, Y. Chen, T. Jiao, J. Zhou, J. Cheng, B. Liu, S. Yang, K. Zhang and W. Zhang, *Adv. Energy Mater.*, 2019, **9**, 1902915.
- X. Qiu, N. Wang, Z. Wang, F. Wang and Y. Wang, *Angew. Chem., Int. Ed.*, 2021, **60**, 9610–9617.
- P. Meister, V. Küpers, M. Kolek, J. Kasnatscheew, S. Pohlmann, M. Winter and T. Placke, *Batteries Supercaps*, 2021, **4**, 504–512.
- L. Zhang, Z. Liu, G. Wang, J. Feng and Q. Ma, *Nanoscale*, 2021, **13**, 17068–17076.
- T. Mandai, *ACS Appl. Mater. Interfaces*, 2020, **12**, 39135–39144.
- G. Pan, J. Li, L. Han, W. Peng, X. Xu, T. Lu, M. A. Amin, Y. Yamauchi, M. Xu and L. Pan, *Inorg. Chem. Front.*, 2022, **9**, 1666–1673.
- N. Wu, W. Yao, X. Song, G. Zhang, B. Chen, J. Yang and Y. Tang, *Adv. Energy Mater.*, 2019, **9**, 1803865.
- H. Ma, H. Chen, Y. Hu, B. Yang, J. Feng, Y. Xu, Y. Sun, H. Cheng, C. Li and X. Yan, *Energy Environ. Sci.*, 2022, **15**, 1131–1143.
- S. He, Z. Mo, C. Shuai, W. Liu, R. Yue, G. Liu, H. Pei, Y. Chen, N. Liu and R. Guo, *Appl. Surf. Sci.*, 2022, **577**, 151904.
- Z. Li, D. Guo, D. Wang, M. Sun and H. Sun, *J. Power Sources*, 2021, **506**, 230197.
- X. Ma, J. Wang, X. Wang, L. Zhao and C. Xu, *J. Mater. Sci.: Mater. Electron.*, 2019, **30**, 5478–5486.
- B. D. Boruah, B. Wen, S. Nagane, X. Zhang, S. D. Stranks, A. Boies and M. De Volder, *ACS Energy Lett.*, 2020, **5**, 3132–3139.
- S. Wang, Q. Wang, W. Zeng, M. Wang, L. Ruan and Y. Ma, *Nano-Micro Lett.*, 2019, **11**, 1–12.



- 30 R. Cui, Z. Zhang, H. Zhang, Z. Tang, Y. Xue and G. Yang, *Nanomaterials*, 2022, **12**, 386.
- 31 J. Shi, S. Wang, Q. Wang, X. Chen, X. Du, M. Wang, Y. Zhao, C. Dong, L. Ruan and W. Zeng, *J. Power Sources*, 2020, **446**, 227345.
- 32 X. Li, M. Li, Q. Yang, H. Li, H. Xu, Z. Chai, K. Chen, Z. Liu, Z. Tang and L. Ma, *ACS Nano*, 2020, **14**, 541–551.
- 33 J. Cao, D. Zhang, X. Zhang, S. Wang, J. Han, Y. Zhao, Y. Huang and J. Qin, *Appl. Surf. Sci.*, 2020, **534**, 147630.
- 34 L. Xu, G. Pan, J. Wang, J. Li, Z. Gong, T. Lu and L. Pan, *Sustainable Energy Fuels*, 2022, **6**, 5290–5299.
- 35 G. Pan, J. Li, L. Han, W. Peng, X. Xu, T. Lu, M. A. Amin, Y. Yamauchi, M. Xu and L. Pan, *Inorg. Chem. Front.*, 2022, **9**, 1666–1673.
- 36 Y. Ding, S. Zhang, J. Li, Y. Sun, B. Yin, H. Li, Y. Ma, Z. Wang, H. Ge and D. Su, *Adv. Funct. Mater.*, 2022, **2210519**.
- 37 H. Zhang, K. Ye, K. Zhu, R. Cang, X. Wang, G. Wang and D. Cao, *ACS Sustainable Chem. Eng.*, 2017, **5**, 6727–6735.
- 38 Z. Li, K. Xiang, W. Xing, W. C. Carter and Y. M. Chiang, *Adv. Energy Mater.*, 2015, **5**, 1401410.
- 39 M. Tian, R. Li, C. Liu, D. Long and G. Cao, *ACS Appl. Mater. Interfaces*, 2019, **11**, 15573–15580.
- 40 J. Yang, M. A. Bissett and R. A. Dryfe, *ChemSusChem*, 2021, **14**, 1700–1709.
- 41 J. Wu, R. Liu, M. Li, X. Luo, W. Lai, X. Zhang, F. Yu and Y. Chen, *J. Energy Storage*, 2022, **48**, 103996.
- 42 X. Zhang, X. Tian, Y. Song, J. Wu, T. Yang and Z. Liu, *Fuel*, 2022, **310**, 122485.
- 43 S. Moon, S. M. Lee, H. K. Lim, H. J. Jin and Y. S. Yun, *Adv. Energy Mater.*, 2021, **11**, 2101054.
- 44 X. F. Ma, H. Y. Li, X. Zhu, W. Ren, X. Zhang, J. Diao, B. Xie, G. Huang, J. Wang and F. Pan, *Small*, 2022, **18**, 2202250.
- 45 Y. I. Kim, B. Kim, J. Baek, J.-H. Kim and J. Yoo, *J. Electrochem. Soc.*, 2022, **169**, 120521.
- 46 W. Han, G. Liu, W. Seo, H. Lee, H. Chu and W. Yang, *Carbon*, 2021, **184**, 534–543.
- 47 X. Li, Y. Li, S. Xie, Y. Zhou, J. Rong and L. Dong, *J. Chem. Eng.*, 2022, **427**, 131799.
- 48 L. Dong, W. Yang, W. Yang, H. Tian, Y. Huang, X. Wang, C. Xu, C. Wang, F. Kang and G. Wang, *J. Chem. Eng.*, 2020, **384**, 123355.
- 49 H. Zhang, Z. Chen, Y. Zhang, Z. Ma, Y. Zhang, L. Bai and L. Sun, *J. Mater. Chem. A*, 2021, **9**, 16565–16574.
- 50 P. Shang, M. Liu, Y. Mei, Y. Liu, L. Wu, Y. Dong, Z. Zhao and J. Qiu, *Small*, 2022, **18**, 2108057.
- 51 F. Wei, P. Xu, C. Xu, M. Han, S. Ran and Y. Lv, *Solid State Ionics*, 2022, **28**, 1419–1426.
- 52 H. He, J. Lian, C. Chen, Q. Xiong and M. Zhang, *J. Chem. Eng.*, 2021, **421**, 129786.
- 53 B. D. Boruah, A. Mathieson, B. Wen, C. Jo, F. Deschler and M. De Volder, *Nano Lett.*, 2020, **20**, 5967–5974.
- 54 P. A. Maughan, N. Tapia-Ruiz and N. Bimbo, *Electrochim. Acta*, 2020, **341**, 136061.
- 55 X. Zhang, C. Chen, S. Gao, X. Luo, Y. Mo, B. Cao and Y. Chen, *J. Energy Storage*, 2021, **42**, 103037.
- 56 G. Lou, G. Pei, Y. Wu, Y. Lu, Y. Wu, X. Zhu, Y. Pang, Z. Shen, Q. Wu and S. Fu, *J. Chem. Eng.*, 2021, **413**, 127502.
- 57 P. Pattananuwat, R. Pornprasertsuk, J. Qin and S. Prasertkaew, *RSC Adv.*, 2021, **11**, 35205–35214.
- 58 N. S. Shaikh, N. S. Padalkar, V. C. Lokhande, T. Ji, S. P. Patil, S. R. Sabale, H. M. Shaikh, J. S. Shaikh, S. Praserthdam and P. Kanjanaboos, *Energy Fuels*, 2022, **36**, 7186–7193.
- 59 K. Shang, Y. Liu, P. Cai, K. Li and Z. Wen, *J. Mater. Chem. A*, 2022, **10**, 6489–6498.
- 60 J. N. Ramavath, M. Raja, K. Balakumar and R. Kothandaraman, *J. Electrochem. Soc.*, 2021, **168**, 010538.
- 61 G. Chen, Z. Hu, Z. Pan and D. Wang, *J. Energy Storage*, 2021, **38**, 102534.
- 62 X. Zhu, F. Guo, Q. Yang, H. Mi, C. Yang and J. Qiu, *J. Power Sources*, 2021, **506**, 230224.
- 63 T. Xiong, Y. Shen, W. S. V. Lee and J. Xue, *Nano Mater. Sci.*, 2020, **2**, 159–163.
- 64 X. Zhang, Y. Zhang, H. Zhang, Y. Zhang, Z. Ma and L. Sun, *ChemistrySelect*, 2021, **6**, 6937–6943.
- 65 L. Yang, J. Li, Y. Zhou and J. Yao, *J. Energy Storage*, 2022, **50**, 104252.
- 66 H. Xu, W. He, Z. Li, J. Chi, J. Jiang, K. Huang, S. Li, G. Sun, H. Dou and X. Zhang, *Adv. Funct. Mater.*, 2022, **32**, 2111131.
- 67 L. Zhang, G. Wang, J. Feng, Q. Ma, Z. Liu and X. Yan, *ChemElectroChem*, 2021, **8**, 1289–1297.
- 68 Y. Wang, L. Zhang, H. Hou, W. Xu, G. Duan, S. He, K. Liu and S. Jiang, *J. Mater. Sci.*, 2021, **56**, 173–200.
- 69 K. D. Benkstein, N. Kopidakis, J. Van de Lagemaat and A. J. Frank, *J. Phys. Chem. B*, 2003, **107**, 7759–7767.
- 70 M. Sevilla and R. Mokaya, *Energy Environ. Sci.*, 2014, **7**, 1250–1280.
- 71 W. Zhang, Y. Song, Y. Wang, S. He, L. Shang, R. Ma, L. Jia and H. Wang, *J. Mater. Chem. B*, 2020, **8**, 3676–3682.
- 72 L. Wei, M. Sevilla, A. B. Fuertes, R. Mokaya and G. Yushin, *Adv. Funct. Mater.*, 2012, **22**, 827–834.
- 73 V. V. Obreja, *Phys. E*, 2008, **40**, 2596–2605.
- 74 Z. Peng, J. Guo, Q. He, S. Li, L. Tan and Y. Chen, *Sci. China Mater.*, 2022, **65**, 1–11.
- 75 M. Zhi, C. Xiang, J. Li, M. Li and N. Wu, *Nanoscale*, 2013, **5**, 72–88.
- 76 C. T. Kingston and B. Simard, *Anal. Lett.*, 2003, **36**, 3119–3145.
- 77 R. Peng, Y. Wang, W. Tang, Y. Yang and X. Xie, *Polymers*, 2013, **5**, 847–872.
- 78 T. Yan, Y. Wu, W. Yi and Z. Pan, *Sens. Actuators, A*, 2021, **327**, 112755.
- 79 H. Zhang, G. Cao, Y. Yang and Z. Gu, *J. Electrochem. Soc.*, 2007, **155**, K19.
- 80 D.-W. Jung, C.-S. Lee, S. Park and E.-S. Oh, *Korean J. Met. Mater.*, 2011, **49**, 419–424.
- 81 K. H. An, K. K. Jeon, J. K. Heo, S. C. Lim, D. J. Bae and Y. H. Lee, *J. Electrochem. Soc.*, 2002, **149**, A1058.
- 82 M. Hughes, G. Z. Chen, M. S. Shaffer, D. J. Fray and A. H. Windle, *Chem. Mater.*, 2002, **14**, 1610–1613.
- 83 Y. Zhang, J. Sun, J. Tan, C. Ma, S. Luo, W. Li and S. Liu, *Fuel*, 2021, **305**, 121622.



- 84 J. Tian, Y. Shi, W. Fan and T. Liu, *Compos. Commun.*, 2019, **12**, 21–25.
- 85 S. Sharma, S. Basu, N. P. Shetti, K. Mondal, A. Sharma and T. M. Aminabhavi, *ACS Sustainable Chem. Eng.*, 2022, **10**, 1334–1360.
- 86 H. Aydın, U. Kurtan, M. Demir and S. Karakuş, *Energy Fuels*, 2022, **36**(4), 2212–2219.
- 87 H. He, J. Lian, C. Chen, Q. Xiong, C. C. Li and M. Zhang, *Nano-Micro Lett.*, 2022, **14**, 1–15.
- 88 H. Xu, W. He, Z. Li, J. Chi, J. Jiang, K. Huang, S. Li, G. Sun, H. Dou and X. Zhang, *Adv. Funct. Mater.*, 2022, 2111131.
- 89 X. Gao, H. Liu, D. Wang and J. Zhang, *Chem. Soc. Rev.*, 2019, **48**, 908–936.
- 90 N. Yang, Y. Liu, H. Wen, Z. Tang, H. Zhao, Y. Li and D. Wang, *ACS Nano*, 2013, **7**, 1504–1512.
- 91 X. Gao, J. Zhou, R. Du, Z. Xie, S. Deng, R. Liu, Z. Liu and J. Zhang, *Adv. Mater.*, 2016, **28**, 168–173.
- 92 N. Parvin, Q. Jin, Y. Wei, R. Yu, B. Zheng, L. Huang, Y. Zhang, L. Wang, H. Zhang and M. Gao, *Adv. Mater.*, 2017, **29**, 1606755.
- 93 I. Hussain, S. Sahoo, M. S. Sayed, M. Ahmad, M. S. Javed, C. Lamiel, Y. Li, J.-J. Shim, X. Ma and K. Zhang, *Coord. Chem. Rev.*, 2022, **458**, 214429.
- 94 M. Yu, W. Qiu, F. Wang, T. Zhai, P. Fang, X. Lu and Y. Tong, *J. Mater. Chem. A*, 2015, **3**, 15792–15823.
- 95 A. Gezović, J. Mišurović, B. Milovanović, M. Etinski, J. Krstić, V. Grudić, R. Dominko, S. Mentus and M. J. Vujković, *J. Power Sources*, 2022, **538**, 231561.
- 96 Y. Liang, H. Dong, D. Aurbach and Y. Yao, *Nat. Energy*, 2020, **5**, 646–656.
- 97 Z. Pan, X. Liu, J. Yang, X. Li, Z. Liu, X. J. Loh and J. Wang, *Adv. Energy Mater.*, 2021, **11**, 2100608.
- 98 N. T. Aristote, X. Deng, K. Zou, X. Gao, R. Momen, F. Li, W. Deng, H. Hou, G. Zou and X. Ji, *J. Alloys Compd.*, 2022, **913**, 165216.
- 99 Y. Liu, B. V. Merinov and W. A. Goddard III, *Proc. Natl. Acad. Sci. U. S. A.*, 2016, **113**, 3735–3739.
- 100 P. Yu, W. Tang, F.-F. Wu, C. Zhang, H.-Y. Luo, H. Liu and Z.-G. Wang, *Rare Met.*, 2020, **39**, 1019–1033.
- 101 L. Dong, X. Ma, Y. Li, L. Zhao, W. Liu, J. Cheng, C. Xu, B. Li, Q.-H. Yang and F. Kang, *Energy Storage Mater.*, 2018, **13**, 96–102.
- 102 K. Zhao, L. Zhao, W. Zhou, L. Rao, S. Wen, Y. Xiao, B. Cheng and S. Lei, *J. Energy Storage*, 2022, **52**, 104910.
- 103 H. Takamatsu, M. S. Khan, T. Araki, C. Urita, K. Urita and T. Ohba, *Sustainable Energy Fuels*, 2022, **6**, 2001–2009.
- 104 R. B. Ambade, H. Lee, K. H. Lee, H. Lee, G. K. Veerasubramani, Y.-B. Kim and T. H. Han, *J. Chem. Eng.*, 2022, **436**, 135041.
- 105 H. Huang, Y. Zhao, T. Cong, C. Li, N. Wen, X. Zuo, Y. Guo, H. Zhang, Z. Fan and L. Pan, *Adv. Funct. Mater.*, 2022, **32**, 2110777.

